

Interstellar Scintillation Observations of 146 Extragalactic Radio Sources

BARNEY J. RICKETT¹

*Department of Electrical & Computer Engineering
University of California San Diego
La Jolla, CA 92093-0407*

T. J. W. LAZIO²

*Remote Sensing Division
Naval Research Laboratory
Washington DC 20375*

FRANK D. GHIGO⁴

*National Radio Astronomy Laboratory
Green Bank
WV 24944*

ABSTRACT

From 1979–1996 the Green Bank Interferometer was used by the Naval Research Laboratory to monitor the flux density from 146 compact radio sources at frequencies near 2 and 8 GHz. We filter the “light curves” to separate intrinsic variations on times of a year or more from more rapid interstellar scintillation (ISS) on times of 5–50 d. Whereas the intrinsic variation at 2 GHz is similar to that at 8 GHz (though diminished in amplitude), the ISS variation is much stronger at 2 than at 8 GHz. We characterize the ISS variation by an rms amplitude and a timescale and examine the statistics of these parameters for the 121 sources with significant ISS at 2 GHz. We model the scintillations using the NE2001 Galactic electron model assuming the sources are brightness-limited.

We find the observed rms amplitude to be in general agreement with the model, provided that the compact components of the sources have about 50% of their flux density in a component with maximum brightness temperatures 10^{11} – 10^{12} K. Thus our results are consistent with cm-wavelength VLBI studies of compact AGNs, in that the maximum brightness temperatures found are consistent with the inverse synchrotron limit at 3×10^{11} K, boosted in jet configurations by Doppler factors up to about 20. The average of the observed 2 GHz ISS timescales is in reasonable agreement with the model at Galactic latitudes above about 10° . At lower latitudes the observed timescales are too fast, suggesting that the transverse plasma velocity increases more than expected beyond about 1 kpc.

Subject headings: ISM: general — scattering — plasmas — galaxies: active — galaxies: quasars — galaxies: BL Lacertae objects

June 19, 2021

¹e-mail: bjrickett@ucsd.edu

²e-mail: Joseph.Lazio@nrl.navy.mil

⁴e-mail: fghigo@nrao.edu

1. INTRODUCTION

Variations in the radio flux density of extragalactic sources have been observed for many decades; see early observations by Dent (1965). Via the classic light travel time argument, variability timescales have been used to infer the physical size of the radio emitting regions, and the associated apparent brightness temperature. Kellerman & Pauliny-Toth (1968) reviewed the early work on centimeter wavelength variations in terms of radiation from (non-relativistic) expanding synchrotron sources. In 1981 the same authors reviewed the topic in the light of very long baseline interferometry (VLBI) observations of apparent superluminal expansion. Since that time a standard picture has emerged of relativistic jets from active galactic nuclei (AGNs), which emit Doppler-boosted radio beams. If the beam points close to the Earth, these are seen as very compact sources with flat radio spectra. The relativistic analysis of such beams successfully explains the sporadic brightenings which emerge from a central core and travel out “superluminally.” In some models the brightenings are thought to be shocks and in others physical structures moving with the jet.

This now canonical jet model has typical Doppler factors in the range 1–20. Flux variations are converted to a “variability brightness temperature,” calculated by the light travel time argument; this increases as the cube of the Doppler factor over the $\sim 10^{12}$ K limit due to inverse Compton scattering (e.g., Blandford & Königl 1979) or over the $\sim 3 \times 10^{11}$ K equi-partition limit as proposed by Readhead (1994). Typical year-long flux variations at centimeter wavelengths give apparent brightness 10^{14} – 10^{15} K, which can be accommodated within the expected range of Doppler factors. However, variations of flux at frequencies below about 1 GHz proved harder to fit in to the jet model. For a source of a given flux density and angular size, the associated brightness temperature scales as the inverse square of the frequency. Thus the observation of substantial variations over a year at a frequency of 0.4 GHz (e.g., Fanti et al. 1981) pushed the apparent brightness to over 10^{16} K and stretched the limits of the relativistic beaming models, by requiring higher Doppler factors to explain the low-frequency variations (LFV)

than to explain the superluminal expansions.

While the discovery of pulsars confirmed that radio sources can vary intrinsically on very short timescales, their flux variations over minutes to hours were quickly found to be due to scintillation caused by inhomogeneities in the interstellar medium (ISM). As reviewed by Rickett (1977) these phenomena were found to be consistent with a very wide range of length scales in the ionized ISM, which causes strong scintillations (rms \gtrsim mean). Dennison & Condon (1981) looked for and set upper limits to such scintillations from a variety of compact extragalactic sources including several LFV sources. The absence of interstellar scintillation (ISS) must be due to quenching by the angular extent of the emitting regions, from which they inferred lower limits to the angular size, which were larger than those inferred from an intrinsic explanation of LFV.

This paradox was resolved by the recognition of a further regime of ISS. At meter wavelengths pulsars show flux variations over days to months as well as over minutes. Sieber (1982) demonstrated that the slower variations were also a propagation phenomenon, which Rickett, Coles & Bourgois (1984) identified as predicted by strong scintillation theory. This is now referred to as refractive interstellar scintillation (RISS) to distinguish it from the diffractive scintillation (DISS) over minutes to hours. Since the angular diameter that quenches RISS is substantially larger than for DISS, these authors proposed that RISS could also account for LFV. The suggestion that LFV was due to irregular interstellar propagation had earlier been made by Shapirovskaya (1978), who proposed that refraction in discrete large scale ionized structures was responsible. Several authors (e.g., Rickett 1986; Spangler et al. 1993) have since demonstrated that RISS does indeed provide a satisfactory explanation for LFV, based on a power-law model for the spectrum in the interstellar plasma density.

A further variability phenomenon at centimeter wavelengths was discovered by Heeschen (1984). In careful daily measurements he found a “flickering” at a level of a few percent over 1–2 days in the radio flux from many flat spectrum sources. The sources which showed the greatest amplitudes were followed up in extensive monitoring campaigns, particularly, by the Bonn group. Quir-

renbach et al. (1992) presented the results of daily monitoring of a complete sample of flat spectrum sources at 6 and 11 cm. They found a low level of what they called intraday variability (IDV) in most of the sources observed, which also had compact VLBI structure. They concluded that this low level of variability seen in almost all such sources was RISS. However, in addition they argued that about 25% of flat spectrum sources also showed intrinsic variations that can reach amplitudes as high as 20%. An intrinsic variation of 0.2 Jy on a timescale of 12 hr implies a variability brightness over 10^{19} K, implying a Doppler factor over 200. Thus for those sources said to be showing intrinsic IDV, flux variations were interpreted in terms extreme brightness emission that strains the limits of the relativistic jet models.

In fact there should be a continuum of ISS behavior between LFV and IDV. The wavelength dependence is determined by a combination of the steep increase with wavelength for the characteristic scale of RISS and the wavelength scaling of effective source diameter. For most extragalactic sources their angular size partially quenches the scintillations and the effective scintillation amplitude and time scale are determined by the compact source size, which scales approximately as wavelength (for brightness temperature limited emission). In an analysis of the flux variations of quasar 1741–038 over a wide range of frequencies, Hjellming & Narayan (1986) identified ISS at a frequency of 1.49 GHz and slower intrinsic variations at 15 and 22 GHz. Dennison et al. (1987) showed that RISS was the dominant cause of the 2.7 GHz variation of two sources at low Galactic latitude, which were in the Green Bank Interferometer monitoring program.

A detailed analysis of one of the large amplitude IDV sources (0917+624) by Rickett et al. (1995) demonstrated that ISS could successfully account for the IDV with a source brightness of about 6×10^{12} K, providing that the scale height of the scattering medium was reduced to 200 pc, from the 500 pc scale height of the Taylor & Cordes (1993) model for the Galactic distribution of electrons. This was one of the sources for which 20% intrinsic IDV had been argued earlier.

An epoch of extremely rapid variability was reported for quasar 0405–385 by Kedziora-Chudczer et al. (1997). They observed large amplitude vari-

ations on timescales as short as one hour at 4.8 and 8.4 GHz. They considered the implied variability brightness 10^{21} K to be unreasonable and argued for an ISS explanation. Rickett et al. (2002) reported detailed analysis of the IDV in the polarization of this source, which they found to be consistent with a maximum brightness temperature of 2×10^{13} K.

Two other quasars have also shown substantial variation over times as short as an hour (intra-hour variation – IHV), namely J1819+385 (Dennett-Thorpe & de Bruyn, 2000, 2002 & 2003) and B1257-326 (Bignall et al. 2003). The measurements of a time delay in the light curves recorded on trans-continental baselines and the observation of annual modulations in their characteristic timescales give irrefutable evidence for scintillation as the cause of the variations for these two quasars. It is also important to note that the three IHV sources mentioned here require that the distance to the scattering medium be only tens of parsecs rather than the 500-2000 pc distances involved in most pulsar ISS. A consensus has finally emerged that the IDV (and IHV) phenomena are due to ISS. The strongest argument in support of intrinsic IDV comes for one particular quasar (0716+714), for which 6 cm IDV was observed to have some correlation in behavior with optical IDV observed simultaneously (Wagner et al. 1996). However, the argument is weakened by the fact that the optical and radio variations were not correlated in detail and there was significant decorrelation across the radio wavelengths observed (see observations by Quirrenbach et al., 2000).

Variations over months and years have been well established at shorter wavelengths, as for example reported by Stevens et al. (1994) who monitored a group of blazars for several years at 22 to 375 GHz. They found reasonable agreement with shock models for the many bursts they observed. They also observed faster variations at lower levels, but the brightness temperature deduced by assuming intrinsic variations are not extreme at their high frequencies.

Most variability studies are based on relatively small samples of sources, often observed at different telescopes using different observing methodologies. Lazio et al. (2001, henceforth L01) presented the light curves and structure functions

for a sample of 146 compact radio sources monitored at the Green Bank interferometer (GBI) over long durations (3–15 yr) with frequent flux density measurements and a common observing methodology. They concluded that the rms variation in flux density at both frequencies was dominated by slow large amplitude changes, due mostly to intrinsic variability on timescales from a few months to a few years. They also found more rapid variations on timescales of 5–50 days, which they characterized as being ISS.

This paper reports further analysis of the GBI flux monitoring program. We shall show that the variations at 2.25 GHz do indeed form a continuum with the ISS phenomena in LFV and IDV. The plan of this paper is the following. In §2 we summarize the GBI monitoring program. In §3 we describe our analysis. In §4 we describe a model for the ISS, which we compare with the observations in §5. In §6 we discuss the results for a few sources of particular interest and we give our conclusions in §7.

2. Observations

Flux density observations with the GBI were made nearly daily from 1979–1987 on 46 radio sources, as described by Fiedler et al. (1987b, henceforth F87) and Waltman et al. (1991, henceforth W91). The sample of sources was expanded to 146 and the frequency of observations reduced to once every 2 days during 1988–1996 (L01). Here we summarize the relevant details of the Navy-NRAO GBI monitoring program; for complete details see F87, W91, and L01.

Sources were selected for monitoring on the basis of their known variability in flux density and/or compact structure. Flux densities were obtained at two frequencies in S-band and X-band. Until 1989 August the frequencies were 2.7 GHz (S band) and 8.1 GHz (X band) after which they were changed to 2.25 GHz (S band) and 8.3 GHz (X band) when new cryogenic receivers were installed.

The observations were made on a baseline of 2.4 km and the correlated flux density estimated from 15 min. integrations of 35 MHz bandwidth summing right and left circular polarizations. Each source was normally observed near the same hour angle each day, but on occasion a single source was observed at multiple hour angles

on the same day. The flux density scale was set by observations of 3C 286.

The typical rms errors in flux density (L01) are, before 1989 August:

$$\sigma_2^2 = 0.037^2 + (0.014S_2)^2 \quad \sigma_8^2 = 0.057^2 + (0.049S_8)^2 \quad (1)$$

and after 1989 August:

$$\sigma_2^2 = 0.0037^2 + (0.015S_2)^2 \quad \sigma_8^2 = 0.0057^2 + (0.05S_8)^2 \quad (2)$$

Here S_2 and S_8 are the flux densities in the S- and X band, respectively.

Attempts to estimate the magnitude of systematic errors suggest that these may approach 10% at S-band and 20% at X-band. There is also a systematic ripple, up to approximately 5% peak-peak in a few sources, introduced by the calibration observations of 3C286. Its origin is unknown (F87), but its 1-yr timescale suggests a seasonally-induced instrumental effect.

Clearly discrepant data were edited out of the published time series by removing those data that deviated by more than 10σ at X band or 15σ at S band from a running boxcar mean. Nonetheless, as can be seen in many of the light curves (L01, Figure 8), there are occasional obvious one-day deviations remaining in the light curves. We do not regard these as valid rapid changes in flux density and we removed them from the time series by a two-step editing process. In each step each data point was compared with a smooth model value obtained from a parabolic fit to a 365-day subinterval centered on that sample. If it deviated by more than 3.5σ it was rejected; here σ is the rms deviation between the data and the model over that subinterval. The rejected points have some influence on the σ and so in a second step the procedure was repeated, rejecting a few more points. With two editing passes the numbers of points rejected from each source in each band were typically 10–30 in 1988–1996 but none in 1979–1987. A few of the rejected points were from the same day at S and X band, which would be due to a common failure in the receiver system or due to a calibration error common to both bands.

We analyzed the data in two sets — 46 sources during 1979–1987 at 2.7 GHz and 8.1 GHz and 146 sources during 1988–1996 at 2.25 and 8.3 GHz. As noted above the second set started with about 18 months at 2.7 GHz. While the frequency change

caused little discontinuity for most sources with relatively flat spectra, there were some for which the frequency change caused a substantial discontinuity in flux density. In such cases we scaled their 2.7 GHz flux densities to 2.25 GHz using the mean spectral index between 2.25 and 8.3 GHz.

After the conclusion of the GBI monitoring program, Fey & Charlot (1997, 2000) quantified the compactness of many of the sources monitored. They determined the contribution of the sources’ structures to interferometric group delays in VLBI observations and characterized the sources by “structure indices” ranging from 1 to 4. A source with a structure index of 1 is relatively compact on scales of order 1 mas, having 90% or more of its flux density in a single component, while a structure index of 4 indicates a relatively extended source, typically having two or more components of approximately equal flux density. The structure indices were listed in Table I of L01 and are used in our analysis below. From models fitted to these and other VLBI observations in S-band we obtained the flux density and diameter of the most compact source component. However, we re-iterate a caution made in L01. It is well known that sources may show structural changes on milliarcsecond scales on timescales of decades. Since the structural estimates are computed from VLBI observations after the end of the GBI monitoring program, they should be taken only as indicators of a source’s structure during the flux density monitoring.

3. Data Analysis

3.1. Methodology

We motivate our analysis by considering the blazar 1514+197¹. Figure 1 shows its light curve from 1988.3 to 1995.3. Immediately evident is that the 2 GHz variations are much more rapid (5–50 days) than the 8 GHz variations, which encompass only three main peaks in 7 yrs. These slow variations also appear at 2 GHz, but with a reduced amplitude and significant delay compared to those at 8 GHz, as expected for intrinsic synchrotron bursts. In contrast, the fast variations are relatively strong at 2 GHz and much

weaker at 8 GHz, which is consistent with the expected decrease in ISS amplitude with increasing frequency. In most of the sources monitored there are 2 GHz variations present on timescales from 5–50 days but at somewhat lower amplitudes than for 1514+197. *Consequently, we adopt the hypothesis that the rapid variations visible in most of the sources at 2 GHz are dominated by ISS and the slower (year-long) variations at both frequencies are intrinsic.* Figure 2 shows a source at a lower Galactic latitude (-11°) with similar behaviour but with a longer timescale at 2 GHz than for 1514+197, which is at latitude 56° .

We separated the fast and slow variations by applying low-pass and high-pass filters to the light curves. For each time series we smoothed the data by a cosine function truncated at its first zeroes with a full width T_{sm} . This smoothed series characterizes the slow variations and was subtracted from the raw series, leaving the difference as the high-pass time series. In the figures the smoothed data are shown by the solid lines and the high-pass time series is simply the deviation of the individual points from the smooth curve. We initially set T_{sm} to 365 days at both 2 and 8 GHz, since typical time-scales for cm-wavelength variations have been a year or more (e.g., Medd et al. 1972; Hughes, Aller & Aller 1992). For a few sources there were substantial slow variations which were nevertheless faster than the 365-day smoothed curve. For these sources we adopted a shorter smoothing time in the range 75–200 days as listed in Table 1. Several of these sources are well-known variables at cm-wavelengths and the separation of intrinsic variations from ISS variations is less clear than for those with intrinsic times-scales of a year or more.

In order to study the scintillation phenomenon in the short term variations, we want to normalize them by the mean intrinsic flux density of each source. Since many of the sources do vary intrinsically, as characterized by the low-pass time series, we divided the high-pass series by the low-pass series for each source. We refer to the result as the scintillation (ISS) data, from which we estimated a timescale and an rms amplitude. For each source we computed the auto-correlation function (acf) at both frequencies and the cross-correlation function (ccf) between them. Though the data were sampled at nominal intervals of either 1 or 2 (sidereal)

¹Throughout the paper we refer to sources by their 1950 coordinates

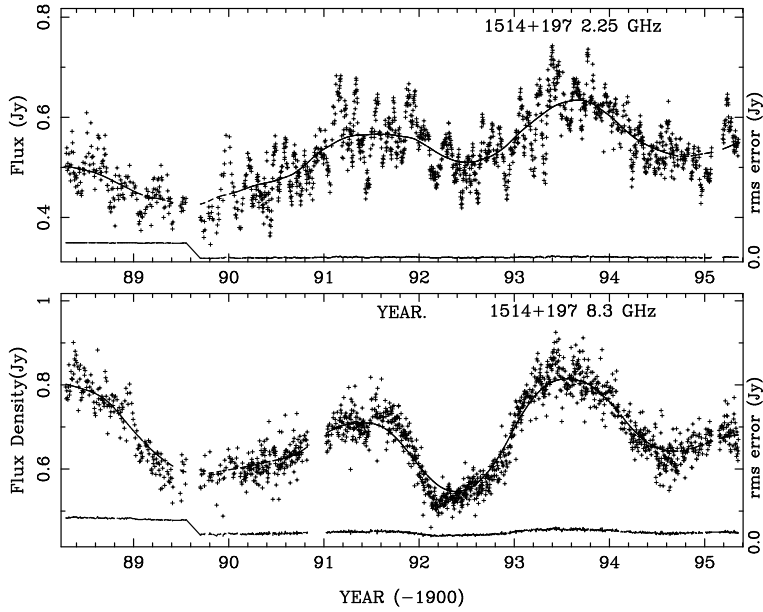


Fig. 1.— Flux density at 2 and 8 GHz for 1514+197. The solid curve is the time series in Jansky smoothed over 365 days with a truncated cosine function. It is interpreted to be dominated by intrinsic variation in the synchrotron radiation from the source. The short term deviations from the line are due to ISS. The trace below each curve gives the rms error in a single measurement (on the same scale) relative to the horizontal axis.

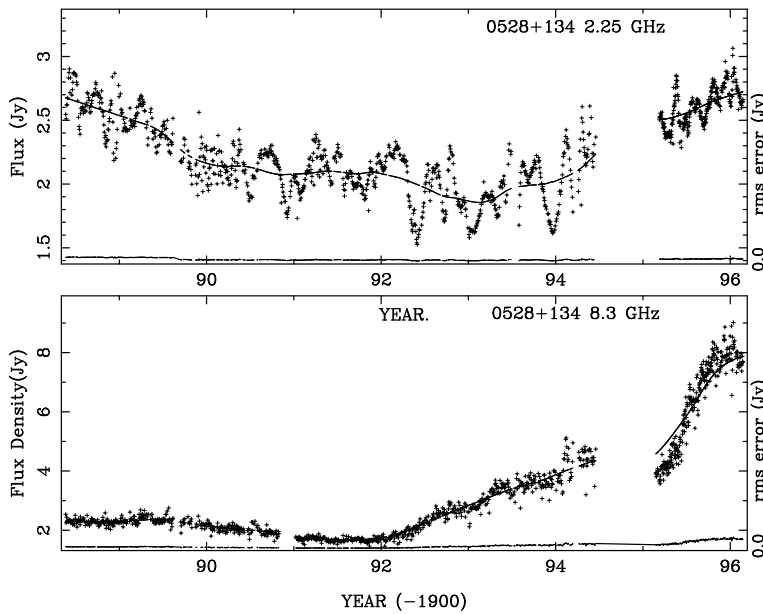


Fig. 2.— Flux density at 2 and 8 GHz for 0528+134 in the same format as Figure 1.

days, the actual sampling is not exactly regular. Thus we computed the acf by summing the lagged products into bins at lags of an integer times the nominal sample interval, normalizing the sum by the actual number of products in each bin. Figure 3 shows examples.

In general the acfs have a narrow spike at the origin, due to noise, a broader component decaying toward zero over times of 5–50 days but typically oscillating randomly about zero at larger lags; superposed on this are noise variations that are independent from one lag to the next. It is the “signal” with a timescale of 5–50 days that we attribute to ISS. We reduced the effect of the noise by smoothing each acf by a Gaussian function with a 3.3 day full width at half-maximum, but first replaced the zero lag point by the acf at the first lag (1 or 2 days). The signal variance was then estimated from this smoothed acf at zero lag. This procedure assumes that the ISS timescale is several days; any rapid (intra-day) variations will not be included in such an estimate but will contribute to the “noise”. The rms amplitude is taken as the square root of this signal variance giving the short-term modulation index $m = S_{\text{rms}}/\langle S \rangle$, since we have already divided by the (varying) source flux density. The signal timescale τ was found as the lag where the smoothed acf crosses half of the signal variance.

This analysis, in principle, allows us to estimate S_{rms} to values well below equation (2), which applies to a single observation of flux density. However, the limit in the equation near $m = 0.015$ is mostly due to uncertainties in the calibration of flux density, which is subject to low amplitude errors – some of them systematic. These may be influenced by weather, equipment changes and other factors that are not well monitored. Thus, even though our m estimates are corrected for the influence of noise and other measurement errors that are independent from one day to the next, we have little confidence in identifying ISS where m is less than about 0.01.

In analyzing the same data, L01 characterized the short-term variability by the logarithmic slope of the intensity structure function computed between lags of 2 and 32 days. They found values between 0 and 1.2, with somewhat higher structure function slopes at lower Galactic latitudes, suggesting that variations on times of 32 days or

shorter were due to ISS. We have plotted this parameter against our modulation index m_2 , and find them to be highly correlated. In general a value of 0.67 is expected for the structure function slope for pure ISS in a Kolmogorov scattering medium that extends up to the observer (see Coles 1988, Blandford, Narayan & Romani, 1986). However, the structure function estimated by L01 was not corrected for the influence of system noise. Since the structure function for pure white noise is flat, the slope parameter will be significantly reduced when the variance due to ISS is comparable to that due to system noise. We use our m_2 estimate to characterize the ISS, since it is corrected for noise. We return to the question of the structure function slope in §5.5.

Table 1 tabulates the results with 1950 coordinates as the source name with Galactic coordinates and effective length through the interstellar plasma (see §4.1). We omit SS433 (1909+048) from the Table and include the Galactic center source Sgr A* (1742–289), but neither are considered in the statistical analyses that follow. We give mean flux densities, modulation index and timescale as m_2 , m_8 , τ_2 and τ_8 at 2 and 8 GHz. The formal errors in these parameters are typically 10-20%, but the acf plots sometimes showed large fluctuations versus time lag. By inspecting each plot we assigned an “ISS confidence level” (0,1,2) at each frequency: 2 is for convincing evidence for short-term variations (errors 10-20%); 1 is for just credible evidence (errors 20-50%); 0 when no credible short-term variations are detected (even though m and τ were formally estimated). This ISS confidence level is given in brackets following the entries for m_2 , m_8 . While at 2 GHz 121 sources show a credible ISS “signal” and a timescale in the range 5–50 days, only 60 sources show credible ISS component at 8 GHz. For the sources observed in 1979–87 as well as in 1988–96, the parameters were estimated separately from each data set. We find a strong correlation (85%) between the two independent estimates of m_2 and somewhat lower correlation (42%) between the two estimates of τ_2 . In Table 1 we list the averages from the two epochs for the 38 sources common to both data sets, and we omit the 5 sources in the first but not in the second data set.

The ccfs were computed in the same fashion but normalized by the square root of the product

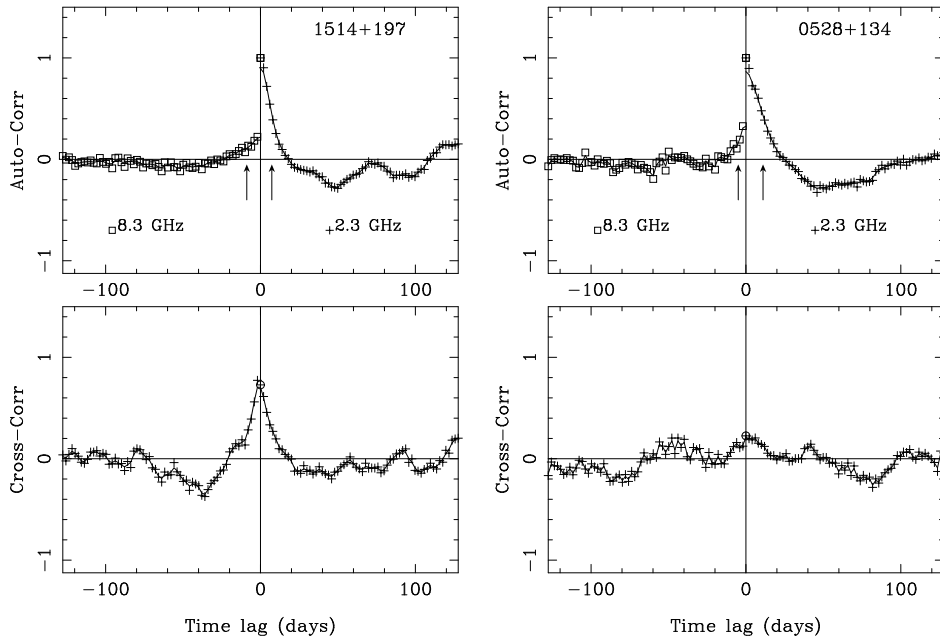


Fig. 3.— Correlation functions for the high-pass filtered time series for 1514+197 (left) and 0528+134 (right) at 2 and 8 GHz. *Top*: Normalized auto-correlations with the 8 GHz acf plotted against negative time lags. The overplotted lines are smoothed as described in the text. The signal variance is found from the zero lag value of the smoothed curve before normalization. The timescale estimates are indicated by vertical arrows. *Bottom*: The cross correlation of the 2 and 8 GHz time series, normalized by the square root of the product of the two signal variances.

of the signal variances at the two frequencies. If the varying signal were fully correlated between 2 and 8 GHz, the two acfs would have the same shape (though perhaps different variances) and the ccf would show the same symmetrical shape peaking near unity at zero lag. Few of the observed ccfs follow such ideal behaviours but typically show random-looking variations over time lags of 10 days or more with superimposed noisy (day-day) variations. Several of the sources with large amplitude slow variations show partial leakage of the intrinsic variation through the high-pass filter; this appears as a cross-correlation peaking at positive lags, which corresponds to 8 GHz variations preceding those at 2 GHz.

It was found also that several sources exhibited a low amplitude spike in the ccf at zero lag. Since these were mostly sources with an ISS confidence level of 0 and 1, the spike is not due to very rapid wide-band ISS. Of course, the additive noise in the time series should be entirely independent at the two frequencies. Thus the spike is an

unexpected correlation introduced perhaps in the calibration process, due to the influence of a temperature change on system gain, bad weather, or some similar systematic effect, which varies independently from day to day. To avoid this influencing our cross-correlation estimates we smoothed the ccfs (ignoring the spikes) in the same fashion as for the acfs and recorded the smoothed ccf at zero lag as a measure of the cross-correlation coefficient. In the table we list this zero-lag correlation coefficient only for the 36 sources with ISS confidence level of two at 2 GHz and one or more at 8 GHz. Among these several cross correlations are influenced by both ISS and relatively rapid intrinsic variations which typically shift the correlation peak to positive time lags, as noted above.

3.2. Overview of Variations

We have completed the analysis described above on all of the sources and have tried to classify their variations, by examining all of their 2 and 8 GHz light curves (see Figure 8 of L01) and

the correlation plots as in Figure 3. In addition to listing the parameters of the short-term variations and the ISS confidence levels, we also list in Table 1 a characterization of the slower variations as M_2 and M_8 , which give the rms variation on a 300-day timescale, normalized by the mean flux density. (This quantity was obtained from the square root of one half of the structure functions of the low-pass time series at a time lag of 300 days for both 2 and 8 GHz).

We find that there are a several types of light curve, that depend on the relative importance of ISS and intrinsic variations. For some sources (e.g., 0235+164, 1749+096, 2200+420) intrinsic variations dominate, showing a sequence of outbursts on times of a few months to 2 yrs, often delayed and reduced in amplitude at 2 GHz relative to 8 GHz, as expected for intrinsic synchrotron flares. For some of these with faster outbursts we needed to reduce the smoothing time T_{sm} (as listed in Table 1), and so the separation of ISS from intrinsic variations is less clear. At 2 GHz many sources show both the long-term (intrinsic) variations and short-term (ISS) variations over 5–50 days. In a few cases (e.g., 1635–035) there is a larger overall amplitude variation at 2 GHz than at 8 GHz. The 2 GHz short-term timescale τ_2 was somewhat longer for sources at lower Galactic latitudes (e.g. 0528+134, 0653–033, 1741–038), but timescales of 20 days were also seen in a few sources at mid-latitudes (e.g. 0537–158, 1614+051, 1635–035). A few sources show the systematic annual variation (e.g., 5% peak-peak for 0952+179), which is also seen at a low level (1.5% peak-peak) in the flux density calibrators 1328+254 and 1328+307.

There has already been considerable analysis of the discrete events known as extreme scattering events (ESEs) in the GBI data (see F87, Fiedler et al., 1994, L01). The complete set of time series in L01 show that there are occasionally other events or evidence of non-stationary variation at 2 GHz. Examples are 1538+149 (see Figure 16) which from 1989.9 until 1991.6 showed a dramatic increase in variation on month-long timescales, and 1502+106 and 2059+034, which both showed several large amplitude excursions which did not meet the criteria for an ESE. The fact that these “events” were much stronger at 2 GHz than at 8 GHz suggests an origin in changing interstellar

propagation conditions, but we do not pursue their origin further.

4. Modeling Interstellar Scintillations and Intrinsic Source Structure

We now develop a model for the expected ISS of the sources in the GBI monitoring program. There are two aspects to this modeling, the ISS itself and the intrinsic source structure. We discuss each in turn, but put the mathematical details of the ISS in Appendix A.

4.1. Interstellar Scintillation Model

From pulsar observations it is known that the ionized ISM has a disc-like Galactic distribution. The electron density microstructure is well-modeled by a power-law power spectrum with a Kolmogorov spectral index on many lines of sight (Armstrong, Rickett, & Spangler 1995). Taylor & Cordes (1993, hereafter TC93) developed a detailed model for the electron distribution in the ISM, which has been revised by Cordes and Lazio (2005, hereafter CL05). Both papers give an explicit model for the local mean electron density and the strength of its small scale variability as characterized by the strength parameter C_N^2 . This parameter sets the level of the density spectrum, $P_{3N} = C_N^2 \kappa^{-11/3}$, at three-dimensional wavenumber κ . In this expression the inhomogeneities are described as isotropic, since along a given line of sight any anisotropies in the density structures are expected to be randomly oriented, so that the cumulated effect is approximately isotropic in the transverse plane. A measure of the cumulated scattering expected for a particular radio source is given by the scattering measure defined as the line of sight integral $\text{SM} = \int C_N^2 dl$. Though the spectral index of the density power spectrum is near $-11/3$ for many lines of sight, C_N^2 and SM can vary by orders of magnitude over angular scales of a few degrees.

There are several observable scattering effects, of which we are concerned with the variability in apparent radio flux density (scintillation). Scintillation is classified as weak or strong according to the scintillation index ($m_{\text{pt}} = \text{rms}/\text{mean flux density}$) for a point source, which depends on the observing frequency as well as on the scattering measure. If $m_{\text{pt}} \geq 1$, the scintillations are strong; if

$m_{pt} \ll 1$, the scintillations are weak. The inverse-frequency dependence of the refractive index in a plasma leads to a decrease in the strength of scattering with increasing frequency.

Interstellar scintillation was first observed in pulsars at relatively low radio frequencies (0.1–1 GHz) and was mostly in the strong regime, in which there are two branches of the phenomenon, diffractive and refractive scintillation (DISS and RISS as already referred to). The extremely small diameters of the emitting regions in pulsars ensures that they scintillate essentially as point sources showing both branches. See reviews by Rickett (1990) and Narayan (1992) for discussions of the physics of DISS and RISS. Given the TC93 distribution Walker (1998, 2001) calculated the transition frequency separating weak from strong scattering for extragalactic sources; he found values ranging from about 6 GHz toward the Galactic poles to about 2 GHz for directions toward the inner Galactic plane.

In contrast, extragalactic sources are observed typically at higher frequencies (2–15 GHz) and in addition their angular extent is much larger than that of pulsars. As a result extragalactic sources are often observed under weak ISS conditions; however, ISS is usually not detectable, because their angular extent is usually sufficient to “quench” the scintillations, in the same way that the angular extent of planets quenches their optical twinkling in the Earth’s atmosphere. These effects explain the rarity of ISS observed for extragalactic radio sources. Low-frequency variability below 1 GHz (§1) is due to strong RISS of compact radio sources (e.g. Rickett, 1986) while IDV is weak ISS (WISS).

The spatial character of the scintillations in a transverse plane can be characterized by the auto-correlation of the intensity (fourth moment of the field) or from its two-dimensional Fourier transform versus transverse wavenumber (the intensity spectrum). From the theory of wave propagation in random media (e.g., Ishimaru 1978), we can obtain a theoretical expression for the intensity second moment, but its evaluation is difficult under the most general conditions. However, the expansion for low wavenumbers leads to the solution for both weak ISS (WISS) and for RISS in strong scattering; the DISS solution is obtained in the high wavenumber limit (see Coles et al. 1987, hereafter

CFRC). When the source has a significant angular extent the fine-scale (high wavenumber) fluctuations of the pattern are smeared out by the effects of overlapping patterns from neighboring source components. This explains why no DISS has been observed from any extragalactic sources (Dennison & Condon 1981). It also means that we only need the low-wavenumber expansion to describe both WISS and RISS. In this limit the intensity spectrum is given by a line of sight integral of the product of the local density spectrum, the Fresnel filter that suppresses the power at low wavenumbers and a low-pass cut-off due to the visibility of the source (CFRC, equation 11).

Rickett et al. (1995) used this method, to interpret the ISS from IDV source 0917+624 observed at frequencies both above and below the weak/strong transition frequency (see also the analysis of IDV from quasar 0405–385, Rickett et al. 2002). Here we follow the same method but generalize the theory to an arbitrary distribution of scattering along the line of sight. In Appendix A we give details of the appropriate expression for the spatial correlation function of intensity as an integral over the distance z from the Earth including $C_N^2(z)$ from the TC93 or CL05 models.

The equations as given in Appendix A yield the scintillation index m_{iss} and spatial scale s_{iss} , under an assumed form for the source visibility function as described in the next section. We convert the spatial scale to a temporal scale by dividing by an assumed velocity for the scintillation pattern. There are a few examples of IDV in which the relevant velocity has been shown to be consistent with the speed of the Earth relative to the local standard of rest (LSR). Consequently we used the annual average of this LSR speed projected transverse to each line of sight as the model velocity (20–30 km s⁻¹), and so obtained model time-scales τ_{iss} for each source. As Appendix A shows, the contribution of the scattering medium to the ISS is controlled by the effective scattering length L_{eff} and the scattering angle θ_s . In developing the necessary code for the calculations we made use of the subroutines described by TC93 and CL05.

4.2. Intrinsic Source Structure Model

Having specified a model for the scattering medium, we must also specify a model for the

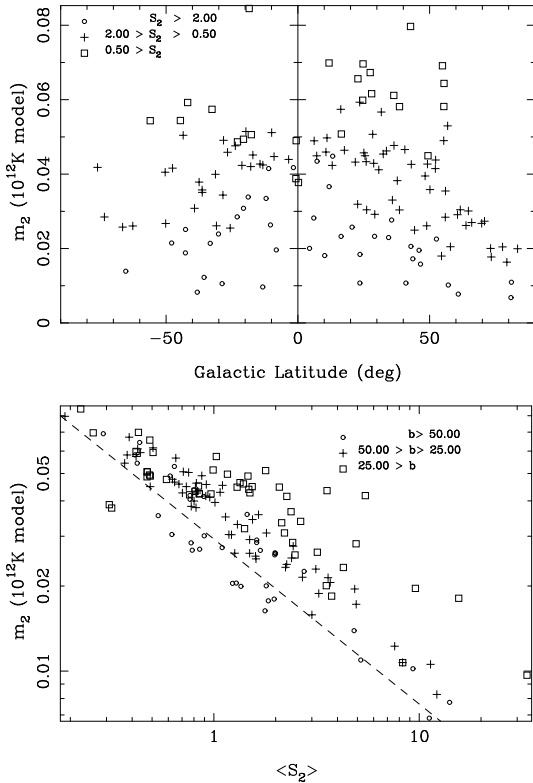


Fig. 4.— Model scintillation index at 2.25 GHz computed under the CL05 model for the Galactic electrons, assuming that each source has 50% of its flux density in a Gaussian core of 10^{12} K brightness. Model scintillation index versus *Left*: Galactic latitude and *Right*: mean flux density with dashed line $m_{\text{iss}} \propto \langle S \rangle^{-7/12}$.

visibility functions for the sources in the survey. Readhead (1994) has argued that the distribution of brightness temperatures from relativistically beamed jets of 5 GHz-selected radio sources ranges from $\sim 3 \times 10^{10}$ to 3×10^{12} K. Accordingly, we adopt a simple model in which the most compact component of each source has a circular Gaussian brightness distribution in which the peak brightness is limited to some maximum due, for example, to synchrotron self absorption or inverse Compton losses. Brightness temperatures up to about 20 times greater than the equi-partition value of 3×10^{11} K are seen in VLBI images of many radio-loud active galactic nuclei. These are well described by relativistic beaming from narrow jets with Doppler factors up to about 20. Thus we

examine three source models with peak brightness temperatures of 10^{11} , 10^{12} , and 10^{13} K. For each of the 146 sources, we assumed 50% of their flux density to come from a Gaussian brightness core of these three temperatures. Hence we obtained three diameters (full width at half maximum – FWHM) using

$$\theta_{\text{FWHM}} = (1.1/f_{\text{GHz}})\sqrt{S_{\text{Jy}}/T_{\text{b},12}} \text{ mas} \quad (3)$$

where the core flux density is S_{Jy} , the peak brightness temperature is $T_{\text{b},12}$ in units of 10^{12} K and θ_{FWHM} is in mas.

Figure 4 shows the computed m_{iss} at 2.25 GHz for the 10^{12} K source models under the CL05 model for the electron distribution versus Galactic latitude and total mean source flux density $\langle S \rangle$. There is only a weak trend for increased m_{iss} at low latitudes; this illustrates its dependence on properties of both the ISM and the source. The right panel shows a lower envelope to the (inverse) relation of m to $\langle S \rangle$. It is approximated by the dashed line, whose slope is from CFRC (equation 13), which with $\theta_{\text{so}} \propto \sqrt{\langle S \rangle}$ gives $m_{\text{iss}} \propto \langle S \rangle^{-7/12}$.

5. 2 GHz Observations Compared with ISS Model

In this section we confront the model with the observations. We begin with global comparisons of the observations with ISS predictions from the model. Next we compare the fast variations to the slow variations, since both the fast ISS and slow intrinsic variations are indicators of compact structure. Finally, in a limited number of cases where the ratio of the ISS signal to the noise is sufficiently strong, we perform two further analyses. First we do a power spectrum analysis and compare with theory. Second we epoch-average the timescale separately for each of the 12 months in the year, in a search for an annual modulation in the ISS timescale due to the changing Earth velocity as it orbits the Sun relative to the scattering medium.

5.1. A Global Comparison for Scintillation Index

Since the short-term variations are much stronger at 2 than at 8 GHz, we compare the modulation indices m_2 and timescales τ_2 with the

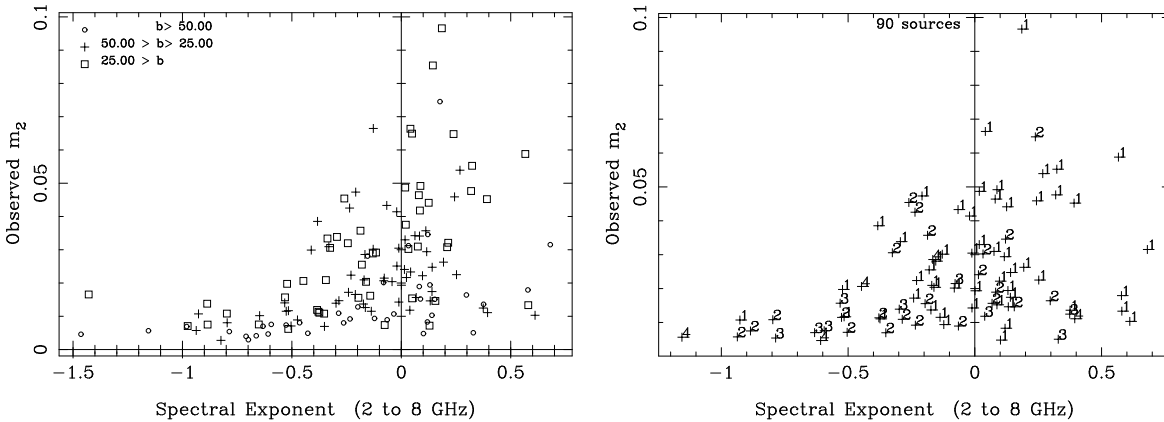


Fig. 5.— Scintillation index at 2 GHz against mean spectral index between 2 and 8 GHz. *Left*: The different symbols flag ranges of the magnitude of the Galactic latitude. *Right*: Subset of sources with structure index 1–4, as an indicator of increasing source size.

ISS models. In making the comparison, we must consider the two major influences, which are the source structure and the distribution of the scattering plasma, for which we use the CL05 model. With our simplistic source model (i.e., 10^{12} K component with 50% of the flux density), the results are only meaningful in a statistical sense. In addition the CL05 model only approximates the Galactic distribution of the warm ionized medium and substantial deviations are to be expected on particular lines of sight. In many of the figures that follow we plot the results against a parameter of the scattering model and flag the points according to some measure of the source model, or vice-versa.

Figure 5 plots the observed m_2 against mean spectral index (α) between 2 and 8 GHz ($S \propto \nu^\alpha$), which is also listed in Table 1. We see that for relatively flat spectrum sources (say $\alpha > -0.4$) there is a much higher fraction of sources with scintillation indices above 1%, than for steeper spectrum sources, as expected if steeper spectrum sources have larger diameters. In the left panel the points are flagged by the magnitude of the Galactic latitude ($|b|$), showing the expected trend for greater ISS at lower latitudes. For the steepest spectra ($\alpha < -0.6$) there is little or no significant scintillation, and so in the analysis that follows we exclude the 17 steep spectrum sources ($\alpha < -0.6$), which include the flux density calibrators.

The right panel shows the subset of sources with

VLBI-observed structure index. The sources with structure indices of 1 or 2 have mostly flatter spectra than those with more extended structure. Also many of the compact structure sources show scintillation indices above 2%. While a structure index of 1 or 2 does imply a small diameter, we note that structure index is defined as a measure the simplicity of a source’s fine structure, that is partially resolved in VLBI; larger structure indices indicate complex structures which can confuse the use of VLBI observations for geodetic purposes. Thus it is not a simple measure of source angular diameter nor of the flux density in a source that is unresolved in a VLBI observation. We have also examined a similar plot flagged by the VLBI model source diameters mentioned in section 2, but there is not a clear trend of m_2 with these diameters.

Figure 6 compares the observed scintillation indices directly with those predicted from the 10^{11} K and 10^{12} K models. In this and subsequent figures, except where noted, we include only those sources with 2 GHz ISS confidence levels of 1 and 2 and spectral index $\alpha > -0.6$. The left panel shows that the 10^{11} K model correlates weakly with the observations, with observed m_2 values lying mostly above the predictions. Note that more sources with flat or inverted spectra tend to lie on the high side of the prediction, as expected. In the right panel the observed m_2 values lie mostly below the predictions for the 10^{12} K model. We conclude that typical brightness temperatures for

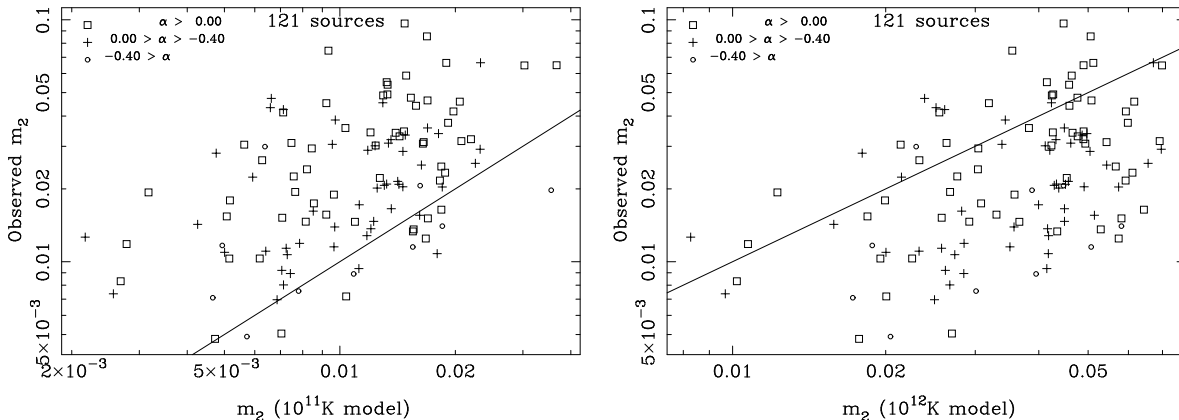


Fig. 6.— Observed ISS index at 2 GHz plotted against the model predictions. In the two models shown half of each source flux density is assumed to be a Gaussian “core” whose peak brightness is 10^{11} K and 10^{12} K on the left and right, respectively. The points are flagged by spectral index as indicated.

the sources are in the range 10^{11} K– 10^{12} K.

The lack of a tight correlation is presumably due to departures from our simple source model. One cause of scatter would be a distribution in the fraction of flux density in the compact core. Consider the effect of a brighter core with a smaller diameter (following equation 3). This would increase the scintillation index, but in order to match an observed S_{rms} and fixed parameters of the scattering medium, we would need a reduced flux density in the compact core. Quantitatively, an observed m_2 compatible with 50% flux density in a 3×10^{11} K component could also be modelled as 3×10^{12} K component with about 5% of the total flux density, providing that the source diameter remains large enough to partially quench the scintillations. For a source small enough to scintillate like a point source the lowest value for S_c becomes equal to the observed S_{rms} which is also a few percent of the total.

The left panel of Figure 7 shows m_2 as a function of Galactic latitude, flagged according to α . There is a generally similar dependence of m_2 on b as in the model of Figure 4. Again the influence of source diameter is shown by the trend for more flat spectrum sources to have higher m_2 values. We examined a similar plot for the 56 sources with credible values for m_8 but it showed only a slight dependence on latitude. The right panel shows m_2 plotted against I_α , where I_α is the intensity of the H_α emission as observed by the Wisconsin

Hydrogen Alpha Mapper in the one degree beam nearest that direction (Haffner et al., 2002). I_α (integrated over -80 to 80 km s^{-1}) is measured in Rayleighs and can be interpreted as proportional to the emission measure in the warm ionized ISM (1 Rayleigh corresponds to an emission measure of about 2.25 cm $^{-6}$ pc at about 8000 K); thus it is an independent measure of the column integrated electron density squared. There is a clear trend of increasing m_2 with I_α , and the trend is strongest for the most compact sources (flat or inverted spectra shown as squares). The dashed line $m_2 \propto \sqrt{SM} \propto \sqrt{I_\alpha}$ gives the theoretical relation if emission measure is proportional scattering measure SM. This applies if the electron density spectrum follows a power law with an outer scale which determines the density variance, which in turn is proportional to the square of total electron density (see CL05 for example). The dashed line is placed to approximate the apparent upper limit line for m_2 .

Figure 8 shows the influence of $\langle S \rangle$ on m_2 . There is a deficit of points in the upper right and lower left of Figure 8, but we do not see the strong inverse relation of m_2 and $\langle S \rangle$ visible in the model of Figure 4. This suggests only a weak influence of $\langle S \rangle$ on source diameter. Is this due to errors or due to inadequacies of the model? The dotted line is the single point error (normalized by $\langle S \rangle$) from equation (2). Though in an ideal observation one could detect variations well below this line, as

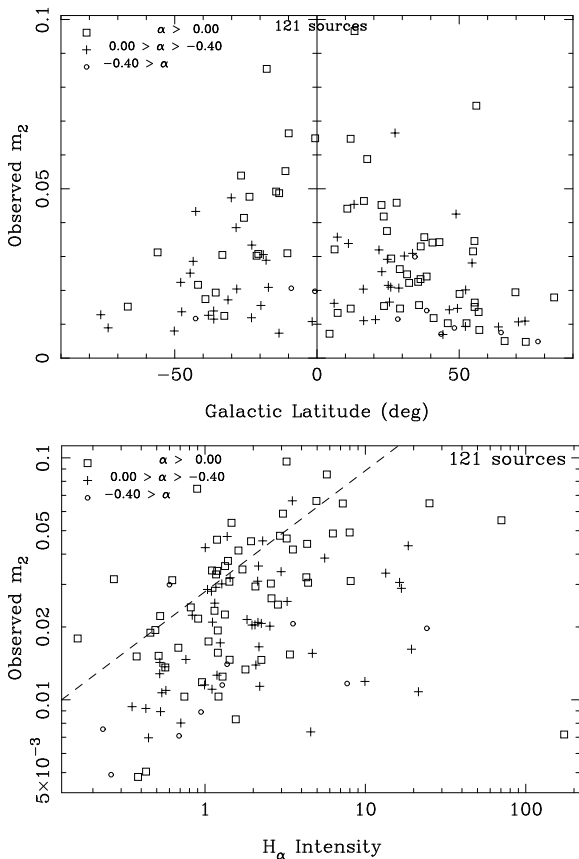


Fig. 7.— Scintillation index at 2 GHz (for sources with ISS confidence levels 1 and 2) plotted against *Left*: Galactic latitude and *Right*: $H\alpha$ intensity (I_α in Rayleighs) as explained in the text. The points are flagged by spectral index as indicated. The dashed line corresponds to $m \propto \sqrt{I_\alpha}$.

noted in §3.1 we consider a lower limit for a credible m value to be $\sim 1\%$. Since the observations extend up to nearly 10%, most of the points are not much influenced by errors. The spread must be caused by a combination of the range of scattering conditions, as indicated approximately by the Galactic latitude and the range of actual source brightness. The dashed line is $m_2 \propto \langle S \rangle^{-7/12}$ from figure 4, which approximates the 10^{12}K model. As noted earlier it is likely that there is a wide range in the fraction of the total flux density in the compact (scintillating) components, which contributes to the scatter about this inverse relation of m_2 and $\langle S \rangle$.

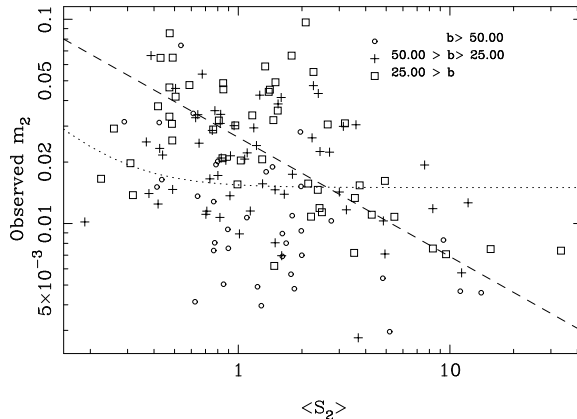


Fig. 8.— Scintillation index observed at 2 GHz against mean source flux density. The different symbols flag ranges of the magnitude of the Galactic latitude. The dotted line is from equation (2) and the dashed line is the rough lower limit for the 10^{12}K model from Figure 4.

In Table 1 we list the flux density and FWHM diameter of the most compact component derived from model fits 2.4 GHz VLBI observations. This gives compact structural information on 93 of our sources (with diameters from 0.3 mas to 8 mas). We tried these values in place of the brightness-limited models to calculate m_2 and τ_2 . Figure 9 shows the observed m_2 versus this prediction, flagged by the FWHM θ_2 . Most of the predicted m_2 values are larger than observed; but for the diameters larger than about 2 mas the observations approximately follow with the predictions. A scatter plot of the 93 VLBI diameters against flux density shows no inverse relation expected if the structures were brightness-limited. It seems that extracting the single most compact component in model fits to VLBI data is not the best way to extract compact structural information for comparison with scintillation data, since sources typically show structure on a range of scales. We conclude that the 2.4 GHz VLBI observations are of limited utility, except for the more resolved sources.

5.2. A Global Comparison for scintillation timescale

We now consider the 2 GHz ISS timescale τ_2 . Figure 10 shows observed τ_2 as a function of b in the left panel. Whereas there is clear increase in τ_2 at low latitudes, the increase is much less than

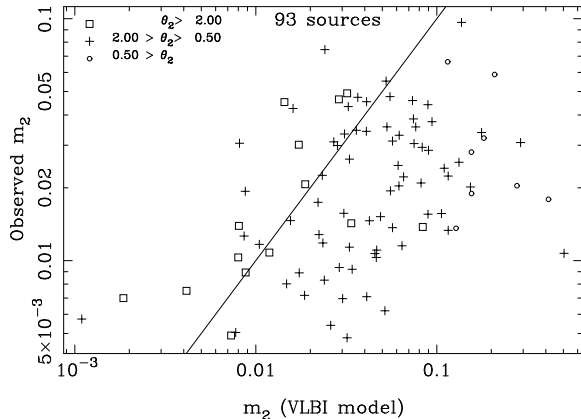


Fig. 9.— Observed m_2 against predicted from the ISS model using source data from S-band VLBI. The points, flagged according to the source diameters, only show agreement for the larger sources.

for the models, as shown in the right panel which plots the observed against the predicted timescale. At latitudes below about 10 degrees the model timescales rise to more than 500 d, due to the very long scattering length through the inner Galaxy. The timescale τ_{ISS} is given by the spatial scale s_{ISS} divided by the Earth’s velocity with respect to the scattering plasma. In our model we took the velocity to be the yearly average of the Earth’s transverse speed with respect to the LSR. Whereas this may be reasonable for scattering paths out to a few hundred parsecs, it will systematically underestimate the velocity at greater distances, due to the absence of differential Galactic rotation and the peculiar motions of the ionized ISM in the model. This presumably explains at least part of the discrepancy.

Overall, we conclude that the general behaviour of the scintillation index m_2 at 2 GHz is quite well described by the CL05 model of the interstellar electrons with the flat spectrum sources having a substantial fraction of their flux density in regions of $3 \times 10^{11}\text{K}$ peak brightness. Ten times higher brightness is possible only from sources with less than about 5% of their total flux density in the most compact core. Our analysis shows only a weak inverse relation of source size to flux density. Thus the sources must be exhibiting a range of peak brightness temperatures around $3 \times 10^{11}\text{K}$, as could be explained by a spread in their Doppler

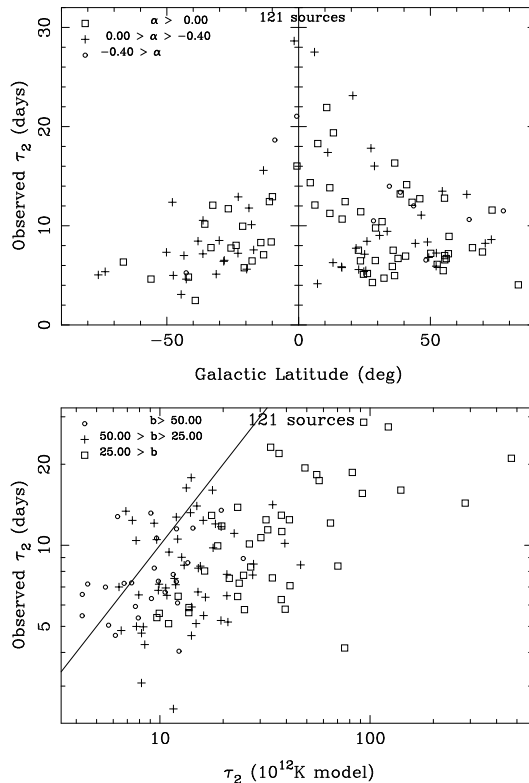


Fig. 10.— *Left*: 2 GHz ISS timescale versus Galactic latitude, flagged for the indicated ranges α . At a given latitude we expect shorter timescales from the more compact sources which typically have higher values of α . *Right*: 2 GHz ISS timescale versus model τ_2 for the 10^{12}K source model, flagged for the Galactic latitude as indicated.

factors.

5.3. Comparison of Fast and Slow Variations

As already noted there are both intrinsic and ISS variations in many of the GBI time series. Indeed the presence of intrinsic (slower) variations was part of the selection criteria for the sample. Since slow intrinsic variations and fast ISS variations are both indicators of compact source structure, we examine the relationship between them.

As described in §3.1 we characterize the low-pass filtered time series by M_2 and M_8 , which are the rms variations on a timescale of 300 days (normalized by the mean flux density), as given in Ta-

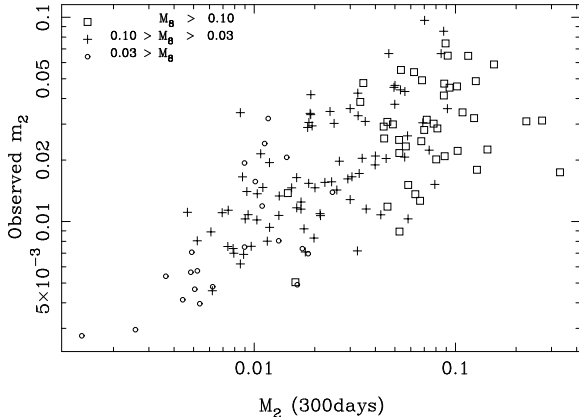


Fig. 11.— 2 GHz comparison of short-term and 300 day modulation indices observed at 2 GHz, flagged by 300 day modulation indices at 8 GHz.

ble 1. We note that these quantities respond to variations on scales of 300-days or longer, including linear trends across the entire data span. Figure 11 shows the 2 GHz ISS index m_2 against M_2 , flagged by M_8 . In this plot we included all the 146 sources, to avoid a bias against low m_2 values for cases where the 2 GHz ISS was not reliably estimated (ISS confidence level 0). The plot shows a strong correlation of the incidence of ISS and intrinsic variations at 2 GHz. This is consistent with both ISS and intrinsic variations being associated with small diameters. The diagram also shows intrinsic variations to be strongly correlated between 2 and 8 GHz as expected.

We also note that Hughes, Aller, & Aller (1992) found time-scales and slopes for the cm-wavelength variation from a set of sources monitored with the 26 m antenna at the University of Michigan. 27 of their sources are in the GBI source list. Their time-scales range from 0.3 to over 3 years, and their structure functions on these time-scales were clustered about 1 year, which they ascribe to intrinsic variation.

5.4. Annual Modulation in ISS time-scale

It has been established that there are annual modulations of the characteristic timescale in several IDV sources (J1819+385, 0917+624, 1257–326 1519–273: Dennett-Thorpe and de Bruyn, 2003; Rickett et al., 2001; Jauncey and Macquart, 2001; Bignall et al., 2003; Jauncey et

al., 2003).

The modulations are due to the annual cycle of the Earth’s velocity relative to the scattering medium. Accordingly, we have looked for similar annual modulations in the ISS signal at 2 GHz. The right panels of Figure 12 show the predicted annual velocity variation for blazar 1514+197.

Our analysis consisted of computing structure functions out to lags of 30 days averaged for each calendar month over all years available. These 12 estimates and their errors are shown by the points in the left panel of Figure 12 for 1514+197. (December is repeated as month 0 and 12). From plots such as this we estimated 12 timescales t_o , by fitting smooth models to each monthly structure function. We first fitted a form to the structure function of the entire time series and selected the best fit as defining the functional form to be used for each month. We tried various forms including an exponential and functions of the form:

$$D_m(\tau) = D_s \frac{t^p}{t^p + t_o^p}. \quad (4)$$

We optimized the parameters D_s , t_o and p (in the range 1.4 to 2.0) and also the exponential (used in place of $p=1$) and selected the best fit. With D_s and p then fixed, we found the best-fitting value of the time scale t_o for each of the 12 months for that source. When available we did independent analyses for the 1979–87 and 1988–96 data sets.

Figure 13 shows some results as nine plots for six sources. The best example is 1514+197 in the lower right panel. The points are t_o and their errors; the lines are predictions ($\propto 1/V_{\text{LSR}}$), assuming that the scattering medium is stationary in the LSR, where the constant of proportionality was set to give one half of the maximum observed t_o for the annual average of V_{LSR} . For 1514+197 there is good agreement between the LSR-model and the observations. See also the right panel of Figure 12. However, for the great majority of the other sources there is not a convincing trend of t_o over the year (relative to the errors); even though, with many years of data, we have as many as 7–8 independent month-long samples for over 100 sources.

There are several factors affecting the analysis. First, the reduced signal-to-noise in one twelfth of the data; second, when $\tau_2 \gtrsim 20$ days there is only one independent “scintle” in each month; third, for low latitude sources the long scatter-

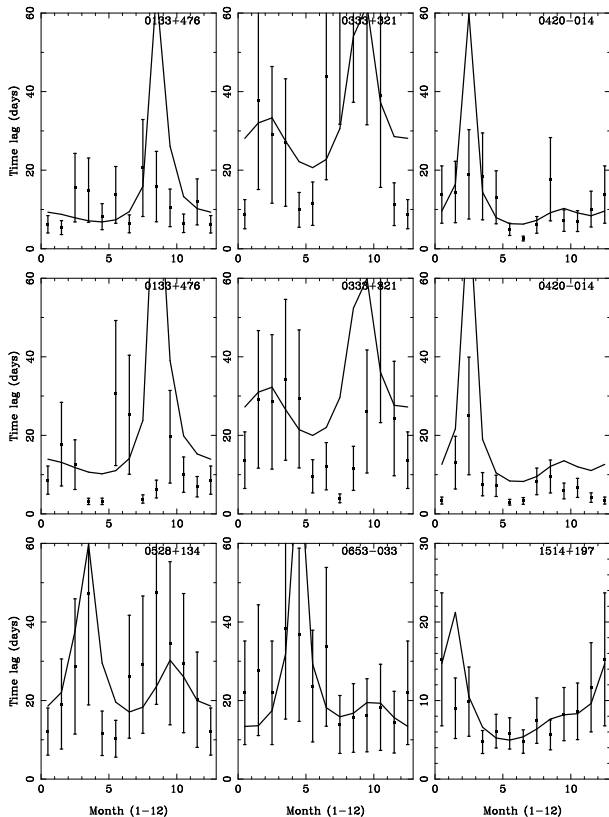


Fig. 13.— Monthly 2 GHz timescale estimates for six sources: top panels from 1979–87; center and bottom panels from 1988–96. Sources 0133+478, 0333+321 and 0420–014 were observed in both periods. The points show observations; the line shows the LSR prediction.

implied using the CL05 model. This difference highlights the importance of refining our knowledge of the electron distribution in the estimation of source structure from ISS.

As mentioned in the introduction variation on timescales as short as one hour are seen from a few extragalactic sources at cm wavelengths. Such rapid variations can only be explained by local scattering “clouds” located 10-30 pc from the Earth. This is in marked contrast to our results reported here in which the CL05 model can successfully explain the 2 GHz variations from 121 compact radio sources. The CL05 model involves scattering at typical distances of 500-1000 pc and has a deficit of electrons in a “local bubble”; thus it specifically excludes scattering in the local ISM.

RISS using NE2001 model $l = 180.0$ $b = 45.0$

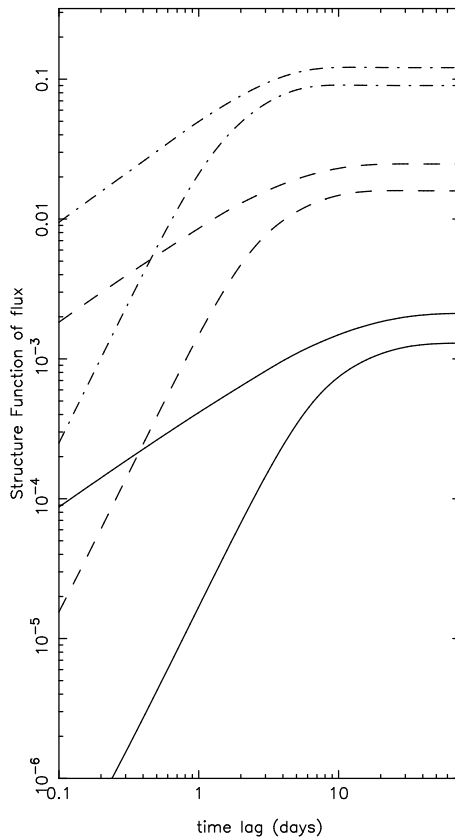


Fig. 14.— Theoretical ISS structure functions for sources with 0.5 Jansky in a Gaussian core of brightness 10^{11} K (solid), 10^{12} K (dashed) and 10^{13} K (dash-dot). Calculations are for 180° Galactic longitude and 45° latitude with the CL05 electron model. The lower steeper curves include a local bubble with much reduced electrons that the electron distribution extends to the solar vicinity.

The importance of this local bubble on the predicted ISS is illustrated in Figure 14. Here the lower curves have reduced scattering plasma in the local bubble (i.e. within about 100 pc of the Sun). Related plots were made by Blandford, Narayan and Romani (1986) and by Coles (1988). The figure shows that observations of the logarithmic slope of the structure can be used to test for scintillation caused in the local ISM; slopes as steep as two are expected when the local bubble eliminates any local scattering, and slopes of

0.67 are expected if the scattering extends to near the Sun. In L01 the slopes estimated from the 2 GHz GBI data were found to lie in the range 0 to 1.2, however, these estimates were not corrected for noise and so cannot be used for this purpose. We do not think that there is a sufficient range of timescales in the data to reliably determine these slopes. The plots of structure function $S_I(T)$ are useful in predicting the apparent scintillation index m in flux density over an observing span T , as $m \sim \sqrt{0.5S_I(T)}$. The differences in Figure 14 largely explain the higher predicted scintillation indices from the TC93 model, which does not model the local bubble.

An important result bearing on the existence of local clouds comes from the MASIV survey reported by Lovell et al. (2003). They observed 710 flat spectrum sources at 4.9 GHz for 72 hours and found 85 with significant variation over that time. However, they only detected one source with variations as fast as 4 hours, which was the well-known IDV quasar J1819+385. The sources surveyed covered most of the Northern sky and so suggest that the covering fraction of local scattering clouds is small (1/85). The GBI observations were not sensitive to ISS on times shorter than one day, but the rarity of time-scales in the range 2-4 d also suggests that the local ISM is indeed depleted of scattering plasma and so supports the local bubble concept.

Another aspect of the three very rapid variables is that detailed modelling of their ISS shows that their local clouds cause anisotropic scattering, i.e. elongated plasma density structures presumably oriented parallel to the local magnetic field. In contrast we assume the scattering to be circularly symmetric in our modelling of the GBI data. Essentially this assumes that the length scale for randomization of the projected magnetic field is substantially smaller than the 500-1000 pc distances through the ISM. However, there is insufficient information in the GBI data to test this assumption. Anisotropy would cause the structure functions (as in Figure 14) to have different widths and shapes in orthogonal directions. These considerations should be included in analysis of any rapidly sampled flux densities in future observations (such as that proposed at the PisGah Observatory).

6. Comments on Individual Sources

We examined plots as in Figures 1 and 3 for all of the 44 sources observed in 1979–87 and the 146 sources observed in 1988–96. Whereas the parameters derived from the correlation analysis are listed in Table 1 and whereas most conform to our hypothesis of rapid ISS at 2 GHz and slower intrinsic variation at 8 GHz, we now discuss some sources which had unusual time series or were otherwise notable. The interested reader is encouraged to peruse the 146 time series plots in L01; where there is also a list of identifications and alternate names for the sources.

Among the sources discussed individually in this section 7 out of 12 are BL Lac objects, compared with 20 BL Lacs among the 146 sources monitored. This may suggest that unusual ISS or unusual intrinsic variations are more common in the BL Lacs than in the quasars, but such behaviour was part of the selection criterion for the observations.

0016+731

This quasar shows obvious variations ($m_2 = 5\%$) on a 1 month timescale at 2 GHz with no slow variations at 8 GHz. The 2 GHz variations appear to be relatively slow ISS; at a latitude of 11° it is near the upper envelope of the τ_2 points in Figure 10. It has a relatively high effective scattering distance of 2.55 kpc and so is probably exhibiting refractive ISS. At 8 GHz there may also be ISS variations on a timescale of 11 d.

0133+476

The quasar 0133+476 is an excellent example of rapid ISS at 2 GHz and year-long intrinsic variations at 8 GHz. It was sampled daily in 1979-86 and every other day in 1988–96. In both 2 GHz data sets there are stochastic variations by 10% on timescales of 10 days; these have much lower amplitudes at 8 GHz but are revealed by cross correlation. The 10-day timescale of its 2 GHz ISS is short considering its Galactic latitude of -14° . The 8 GHz data show 25% variations (presumably intrinsic) on timescales of a year, having a much lower amplitude at 2 GHz.

The BL Lac object 0235+164 is a much-studied variable at many radio wavelengths. Both the 2 and 8 GHz time series are dominated by deep ($M_2 \sim .4$; $M_8 \sim 0.6$) relatively slow variations, which we interpret as intrinsic. The major outbursts over year-long timescales are often accompanied by lower level events on times of a few months. The 2 GHz variations are delayed by 1-3 months, with some evidence that the delay increased between 1982 and 1994. At 2 GHz there are also low level rapid variations particularly near the peaks in the outbursts (e.g. in 1992–93). We presume that these latter were ISS due to the emergence of new components (like those in VLBI images) compact enough to scintillate, which then expanded and quenched the ISS.

In Figure 15 we plot the flux densities overplotted with a 50-day high pass running mean. The middle curve is a running estimate of σ_{iss} , which is the net rms deviation in flux density from a quadratic curve fitted to the 50-day interval centered on each point. At 2 GHz σ_{iss} is well above the lower curve which shows the rms due to noise and estimation error, which has not been subtracted from σ_{iss} . Often the ISS peaks earlier in a burst than does the total flux density, as expected for the ISS of an emerging compact emission feature. A clear example is the major burst during 1992–1993, where σ_{iss} increases abruptly in 1992.7 just as the 2 GHz flux density starts to rise. A simple model for the ISS of such a single transient component of diameter $\theta(t)$ and flux density $S_b(t)$ is

$$\sigma_{\text{iss}} \sim S_b(t)m_o\theta_o/\sqrt{\theta(t)^2 + \theta_o^2}, \quad (5)$$

where θ_o is the critical diameter for suppression of the ISS and m_o is the scintillation index of a point source (~ 1.0 at 2 GHz). The physics of the expanding feature will determine the relation of $\theta(t)$ to $S_b(t)$; while it is optically thick one may expect increasing $S_b(t) \propto \theta(t)^2$ and then a decay in $S_b(t)$ as it becomes optically thin.

The 1992.7 event suggests a very rapid rise in $S_b(t)$ while its diameter $\lesssim \theta_o$. We shortened the time for the running estimate of σ_{iss} to 30-d and made a scatter plot of σ_{iss} against $S(t)$ during the rising part of the burst. This revealed that σ_{iss} rose from 0.06 to 0.12 Jy while $S(t)$ increased from 1.7 to 1.77 Jy. In other words σ_{iss} increased by

0.06 Jy while the flux density increased by 0.07 Jy (both figures have errors of about 25%). Thus 0.07 Jy flux density emerged with a scintillation index of $0.06/0.07 \sim 0.9$ implying a diameter $\lesssim \theta_o$, which we estimate as about $10 \mu\text{as}$ using the L_{eff} tabulated in Table 1. An emission component of 0.07 Jy with a diameter of $10 \mu\text{as}$ at 2.25 GHz implies a remarkably high brightness temperature of about $1.7 \times 10^{14}\text{K}$ during the few days that σ_{iss} showed the rapid rise. Subsequently σ_{iss} remained constant while the total flux density nearly doubled from 1.77 to 3.4 Jy. This suggests a relationship between the effective diameter of the new component and its contribution $S_b(t)$ to the total flux density, but further theoretical work is needed to make a quantitative model of the expansion.

It is notable that Kraus et al. (1999) were monitoring the source at the VLA and observed a peak in the flux density of 0235+164 at 1.5, 4.9 and 8.4 GHz on modified Julian days 8904-8905, coincident with the abrupt increase in σ_{iss} at 2 GHz. They considered both intrinsic and extrinsic explanations, and our analysis suggests the emergence of a very bright component at that time, which contributed to the rapid change in the light curve at 1.5 to 8.4 GHz. However, the subsequent rapid variations of the flux density are clearly strongly influenced by ISS. This event highlights the importance of both phenomena in any detailed interpretation of such outbursts.

Viewed over the full span 1979-1996, the 2 GHz flux density for this source shows 30-50% variations on times of several months combined with only a low average level of ISS ($\sim 2\%$) variation on times of 3 days. This is a lower level of ISS than seen for several sources with very little intrinsic variation (e.g. 0133+476 and 1514+197), and it suggests that even though the source is highly variable the average flux density coming from sub-mas structure is low relative to that in sources which show a higher average value for m_2 .

0355+508

This low latitude ($b = -1.7^\circ$) quasar (NRAO 150) was one of two objects from the 1979–87 observations analyzed for ISS by Dennison et al. (1987). At 2.7 GHz they found a slow decay over 7 yr and 5% variations on times of 1 yr, which they showed is consistent with strong refractive ISS as expected at such a low latitude, quenched

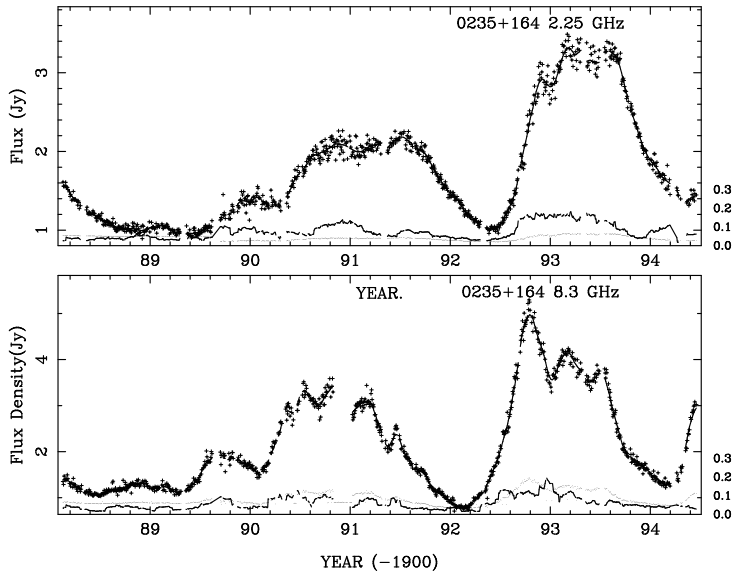


Fig. 15.— Flux density vs time for 0235+164. The middle curve is a 50-day running estimate of σ_{iss} described in the text and the lower curve is the rms error in flux density; both curves scaled times 3 as indicated by scale on the right.

by a 10:1 factor due to the angular diameter of the source which they estimated as 7 mas, which is comparable to the 5 mas listed in Table 1. Even at 8.1 GHz the model predicts refractive ISS for this source.

They made no precise definition of timescale but 1 yr appears to be the “quasi-period” of the variations about a slow decay, suggesting a timescale in our definition of about 6 months. When analyzed through our 365-day high-pass filter we find a time scale of 1-2 months, which illustrates that the use of the high-pass filter to separate ISS and intrinsic variations is only possible when the two timescales are widely different. We detect 3% variations at 8 GHz on a timescale of 13 days, which is comparable to the 25 days predicted in their model.

0528+134

As shown in figure 2, this quasar was quiescent at 8 GHz over 1988–1992. It then started a slow increase about doubling its flux density by 1994. Then over 1995.2–1996.0 it rose to 8 Jy, doubling its flux density again in less than 1 yr. The ISS at 2 GHz is 5% on a timescale of 12 d persisting throughout the 8 years of monitoring. We looked for the associated increase 2 GHz ISS amplitude

as the 8 GHz burst began, as seen in 0235+164. However, though the flux density at 2 GHz did start to increase, the ISS amplitude did not, although it became somewhat faster. This shows that an increase in ISS is not always seen at the onset of an intrinsic burst.

0716+714

0716+714 is a BL Lac object studied extensively by the Bonn group and exhibits IDV at cm wavelengths (e.g. see Quirrenbach et al., 2000). Their structure function analysis shows significant variations on times 2 days at the 1–2% level. at 1.4 and 4.8 GHz. In the GBI program it was mostly sampled at 2 day intervals and shows significant 2.2 GHz variation at about 4.8% rms on a timescale of 5 days.

Wagner et al. (1996) also report a relationship between its optical and radio variations, which they interpret as evidence for intrinsic IDV at cm wavelengths. If as they suggest the 4.8 GHz IDV were intrinsic with a Doppler factor ~ 100 , the observable angular diameter would be $\sim 3\mu\text{arcsec}$. Scaling this to 2.2 GHz, we obtain $\sim 6\mu\text{arcsec}$, which should scintillate as a point source, showing both refractive and diffractive ISS. However, our 2.2 GHz observations suggest refractive ISS only

with possible smoothing by a source diameter of ~ 0.5 mas.

0851+202

Another BL Lac object 0851+202 (OJ287) is similar to 0235+164 in showing vigorous intrinsic variability on timescales of a few months, which is highly correlated between 2 and 8 GHz and only 2.8% rms in ISS at 2 GHz. There are peaks in the short-term rms in 2 GHz flux density at the beginning of the intrinsic bursts, but the evidence is not as strong as for 0235+164.

0954+658

This BL Lac object shows 10-20% variations over a year at 8 and 2 GHz, with the time delay from high to low frequencies characteristic for intrinsic bursts. It is well known since it produced the best and most definitive ESE in 1981 (Fiedler et al., 1987a). Our analysis also shows that it clearly exhibits typical 2 GHz ISS on a timescale of 4 days at 3.4% scintillation index.

1413+135

This BL Lac is remarkable for its strong intrinsic variations (over 25%) at 8 GHz and remarkably low level ISS ($\sim 0.6\%$) at 2 GHz, where it also has only a low level of 300-day variation. Thus it appears as an outlier near the center top of the right panel in Figure 11. This source has an inverted spectrum ($\alpha = 0.33$), making a possible explanation that the compact core is heavily absorbed at 2 GHz and contributes little to the 2 GHz flux density.

1514+197

This BL Lac object shows the highest level of ISS at 2 GHz (7.5% rms on a timescale of 7 d) of all of the extra-galactic sources in the sample. At a latitude of 56° it is expected to be in weak ISS or near the transition frequency. Thus its high level of ISS suggests a smaller diameter than other sources. 2.3 GHz VLBI observations reported by Fey and Charlot (2000) list its structure index as 1 — the most compact but its VLBI-modelled angular diameter in Table 1 is 1.8 mas which is not unusually small. The relatively high level of ISS in this source revealed an annual modulation in its ISS timescale agreeing in phase with that

predicted for a scattering plasma at rest in the LSR. We have computed the power spectrum of its 2 GHz ISS and compared it with predictions for a Gaussian source model, assuming a screen or the CL05 and TC93 models of the ionized ISM. These give agreement in the width at half power of the ISS spectrum for a source diameter ~ 0.25 mas, which corresponds to a brightness temperature of $\sim 10^{12}$ K. As shown in Figure 3 and listed in Table 1, its ISS is also detected at 8 GHz with an amplitude of 2% on a timescale 11 d and is 52% correlated with the 2 GHz ISS. This is the best example of 8GHz ISS in our data.

1538+149

The 2 GHz time series in Figure 16 has an episode of strong variability starting abruptly in 1989.9 and ending abruptly in 1991.6. Before and after this episode there are typical ISS variations at a few percent over 10 days; during the 20-month episode there were about ten excursions of $\pm 25\%$ on time scales of about one month. At 8 GHz there are 10% variations on times of 6 months and during the 2 GHz episode some signs of similar variations at a lower amplitude. The higher amplitudes at 2 GHz strongly suggest ISS as the cause of the 2 GHz episode. Is this due to a change in the source or the medium? While we cannot give a definitive answer, the stochastic appearance and slower than normal timescale (at a latitude of 49°) suggests that an unusual region of enhanced turbulence intervened during 1989.9–1991.6, causing strong refractive variations. The 20-month duration at 30 km s^{-1} implies a size of the region ~ 10 AU.

It is possible that this episode is similar to an ESE, but that the ISM structure was larger including multiple regions with sufficient refracting power to focus or defocus the 2 GHz radiation. Hence we looked at all sources for non-stationary episodes and found unusual 2 GHz variations in 0355+508, 0537–158, 0836+710, 1100+772, 1502+106, 1741–038.

1741–038

Hjellming and Narayan (1986) analyzed one year of observations at 1.5, 5, 15 and 22 GHz of this quasar, which lies at a low latitude (13°) toward the inner Galaxy. They identified 20-d

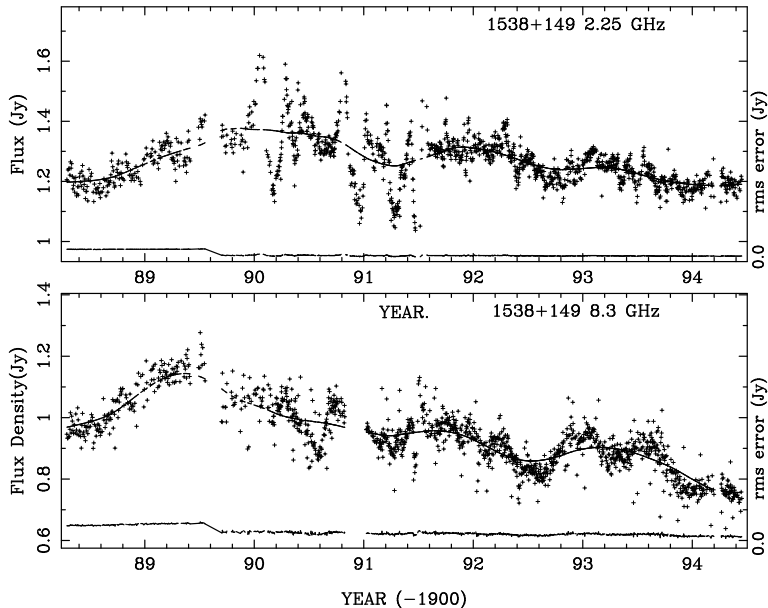


Fig. 16.— Flux density at 2 and 8 GHz for 1538+149 in the same format as Figure 1. Note the episode of enhanced variation at 2 GHz from 1989.9–1991.6, as discussed in §6.

variations at 1.5 GHz as refractive ISS (possibly caused at a few hundred parsecs in the North Polar Spur), while the higher frequencies were dominated by intrinsic variation. Our 2 GHz results also give an 18-d timescale at an rms amplitude of 10%. However, the 2 GHz auto-correlations are strongly influenced by the inclusion of data from a well studied ESE (1992.2–1992.6, see Lazio et al., 2000). During the event the 2 GHz flux density decreased to a minimum 50% of normal, remaining lower than 75% for about 2 months.

Examination of the entire 2 GHz time series reveals $\pm 10\%$ variations on similar timescales from 1983.5–1994.5. There is also a period 1988.0–1989.6 during which the timescale appeared to be much shorter (~ 12 d). The VLBI observations following the minimum in the light curve at 1992.4 showed that the source had a diameter of 0.9 mas during the minimum flux density and 0.6 mas afterwards. Lazio et al. (2000) concluded that the increase in diameter during the event was due to an extra stochastic broadening.

For refractive ISS we expect a timescale $\sim L\theta/1.7V$ for a scattering at distance L of a source observed to have a diameter θ with transverse velocity V . For 0.9 (0.6) mas at 1 kpc and 30 km s^{-1} we obtain 32 (21) d. These are within 50% of

our estimated ISS timescale and suggests that the conditions for the normal ISS and the ESE are fairly similar. However, as noted for several of the sources discussed in this section, there is good evidence for non-stationary behavior in the ISS phenomenon, which is presumably based in distinct physical structures crossing the line of sight on occasion.

2005–403

This quasar lies at 4 degrees latitude in the Cygnus region and is substantially broadened by interstellar scattering. As shown by Desai & Fey (2001) its scattering disc has a diameter of 18 mas at 2.3 GHz with an axial ratio of (0.76:1), and its diameter scales as $(\text{wavelength})^2$. The associated refractive ISS should have a time scale of about 1.1 years and cannot be distinguished from the slow intrinsic variation and (spurious) annual variation visible for this source. However, at 8 GHz there is a 4% variation on a timescale of ~ 12 d, which we suggest is ISS. Extrapolating their diameter measurements to 8.3 GHz gives a scattered diameter of θ_{mas} 1.3 mas. If the intrinsic source size was no larger than this we would expect the ISS timescale to be about $18 \text{ days} \times L_{kpc} \theta_{mas} / (V_{kms}/50)$, where the scatter-

ing path is L_{kpc} and V_{kms} is the transverse velocity of the medium relative to the Earth. The nominal scattering distance is 5.5 kpc, which would only agree with the 12 d timescale if $V_{\text{kms}} \sim 500 \text{ km s}^{-1}$. This is unreasonably high given a 220 km s^{-1} Galactic rotation velocity, and suggests that the effective distance to the scattering plasma is much less than 5.5 kpc. At 1 kpc the timescale implies a transverse velocity of 90 km s^{-1} — still higher than the $30\text{-}50 \text{ km s}^{-1}$ commonly assumed. However, these figures are necessarily crude, since they do not include effects of anisotropic scattering or the distribution of scattering along the path. We also note that the time-series of 8 GHz flux density has several intervals with quasi-oscillatory variations which have timescales noticeably longer than the 12 d derived from the correlation analysis.

7. Discussion and Conclusion

We have used a simple filter on the time series of flux density to separate slow intrinsic variations from fast ISS on all of the light curves from the GBI monitoring program. The results confirm that both processes are widespread and must be considered together in a full description of compact radio sources. Both processes imply small diameters for the sources.

Our model for the interstellar scattering is that it is caused by “turbulence” in the ionized ISM as described by the CL05 model. We also computed the ISS based on the TC93 model which predicted generally slightly higher scintillation indices and about 15% shorter time scales. This was particularly evident in the form of the predicted sstructure function at small time lags.

- We find that a simple filtering can separate the fast ISS from the slow intrinsic variations in flux density at 2 GHz. A demarcation timescale of about 365 d is satisfactory for most of the sources.
- We identify the 5–50 d variation in the 2 GHz flux density of about 121 sources as ISS. These variations are the expected ISS phenomenon intermediate between LFV and IDV.
- The modulation indices and timescales show clear dependence on Galactic latitude. This

confirms that ISS is the origin of such fluctuations. In addition there is a strong correlation of the 2 GHz scintillation index with the emission measure estimated from WHAM H_α emission.

- Over the 121 sources the 2 GHz ISS modulation index is correlated with the mean spectral index and also with the detection of compact structure on VLBI scales.
- A model for ISS in the CL05 (or TC93) medium is reasonably successful if the peak brightness of the compact core of each source is in the range 10^{11}K to 10^{12}K and 10-50% of the source’s flux density is in such a compact component. This is in general agreement with the distribution of brightness temperatures proposed by Readhead (1994).
- There is a weak inverse correlation of scintillation index with mean flux density, as expected if the effective diameter of a source is limited by a maximum in brightness temperature.
- There is a significant population of sources that show substantial 2 GHz ISS, but do not vary intrinsically (above about 4% on times of a year or more). This implies that some very compact sources do not vary intrinsically. Conversely, there are a few 8 GHz sources with strong intrinsic variations with surprisingly low levels of ISS at 2 GHz.
- An annual modulation in the ISS time-scale is found for a few sources, confirming both the ISS model and that in these directions the scattering plasma moves approximately with the local standard of rest. However, most sources do not show such a simple annual cycle, implying that we do not have an accurate understanding of the velocity of the scattering plasma.
- An intrinsic outburst from the BL Lac object 0235+164 was detected in 1992.7 by the sudden onset of ISS at 2 GHz while its total flux density started a steep rise. We estimated the brief emergence of a component as bright as $1.7 \times 10^{14}\text{K}$ which decreased over a few days as it expanded, eventually doubling the total flux density of the source.

- At Galactic latitudes less than about 15 degrees from the plane the ISS model needs to include differential Galactic rotation, which will increase the effective velocity of the ISM relative to the model and so decrease the predicted time-scale. This may include a wide enough velocity range along the line of sight to invalidate the “frozen pattern” assumption.

We thank A. Fey for helpful discussions and for providing the VLBI data. We thank E. Waltman for her many years of work with the GBI, without which both the data quality and quantity would have been much reduced. The Green Bank Interferometer is a facility of the National Science Foundation operated by the National Radio Astronomy Observatory, under contract to the US Naval Observatory and Naval Research Laboratory (NRL) in support of their geodetic and astronomy programs. Basic research in radio astronomy at the NRL is supported by the Office of Naval Research. The National Radio Astronomy Observatory is a facility of the National Science Foundation operated under cooperative agreement by Associated Universities, Inc. The interstellar research at UCSD was partially funded by the National Science Foundation under grants AST 9988398 and 0507713. We thank Bill Coles for valuable discussions and we thank Ron Reynolds for access to the data from the Wisconsin H-Alpha Mapper, which is funded by the National Science Foundation.

A. Intensity correlation for WISS and RISS

In the ISS model of Rickett et al. (1995) a Gaussian function was assumed to describe the dependence of C_N^2 on distance from the Earth; here we use the same basic method, but instead integrate the CL05 or TC93 model in the direction toward each source.

For a source of unit flux density the intensity covariance function (at offset \mathbf{s}) is given by CFRC equation (11), which we rearrange in terms of distance z measured from the observer:

$$C_{\delta I}(\mathbf{s}) = 8\pi r_e^2 \lambda^2 \int_0^\infty dz \int_0^\infty d^2 \mathbf{q} C_N^2(z) q^{-\alpha-2} \times \\ |V(qz/k)|^2 \sin^2\left[\frac{q^2 \lambda z}{4\pi}\right] \exp[-D_r(q, z) + i\mathbf{q} \cdot \mathbf{s}] \quad (\text{A1})$$

Here $k = 2\pi/\lambda$ for wavelength λ , r_e is the classical electron radius, $\alpha = 5/3$ for the assumed Kolmogorov spectrum of density as $C_N^2(z)q^{-\alpha-2}$ at transverse wavenumber q . The refractive cut-off is given by:

$$D_r(q, z) = \int_0^\infty dt D'(q \min(t, z)/k, t) = (qL_{\text{eff}}(z)\theta_s)^\alpha \quad (\text{A2})$$

and $D'(s, z)$ is given by equation (4) of CFRC. The second part of equation A2 involves an effective path length through the scattering medium:

$$L_{\text{eff}}(z)^\alpha = \int_0^\infty dt [\min(t, z)]^\alpha C_N^2(t) / SM \\ SM = \int_0^\infty dt C_N^2(t) \quad (\text{A3})$$

It follows that near the observer the scattering distance is effectively $L_{\text{eff}}(z) \sim z$; but at large distances from the observer L_{eff} saturates at about the 1/e scale of the C_N^2 distribution. The scattering angle θ_s corresponds to the effective angular broadening at the observer:

$$\theta_s = k^{-1} \left[8\pi^2 r_e^2 \lambda^2 SM \frac{\Gamma(1 - \alpha/2)}{\Gamma(1 + \alpha/2)\alpha 2^\alpha} \right]^{-1/\alpha} \quad (\text{A4})$$

We proceed as in CFRC to approximate the exponent α in A2 by a value two in place of 5/3. As this only governs the precise form of the refractive cut-off it changes the result very little. We further assume that the source visibility is a circular Gaussian function:

$$V(u) = \exp[-0.5(uk\theta_{so})^2] \quad (\text{A5})$$

in which the source diameter is $2.35 \theta_{so}$. These two assumptions make a Gaussian cut-off in the wavenumber integral, which allows the integral to be done as in the Appendix of CFRC in terms of a confluent hypergeometric function. We then numerically integrate equation A1 with the TC93 weighting for C_N^2 over z to obtain $C_{\delta I}(\mathbf{s})$.

The modulation index is then given by $m = \sqrt{C_{\delta I}(0)}$ and the spatial scale s_{iss} is found by solving for where the correlation falls to 0.5 of its maximum: $C_{\delta I}(s_{iss}) = 0.5C_{\delta I}(0)$.

TABLE 1
SHORT-TERM VARIATIONS IN GBI FLUX DENSITY MONITORING

Name 1950	l deg	b deg	L_{eff} kpc	S_2 Jy	S_8 Jy	$m_2(\text{rel})$	τ_2 days	T_{sm} days	$m_8(\text{rel})$	τ_8 days	M_2	M_8	ρ	spectral index α	$S_{2,\text{vlbi}}$ Jy	Diameter mas
0003+380	113	-24	1.61	0.59	0.89	0.048(2)	8.0	365	0.044(1)	28.2	0.035	0.126	0.23	0.32	0.61	1.25
0003-066	93	-67	0.68	1.98	2.22	0.015(2)	6.3	365	0.023(0)	19.7	0.079	0.091	-	0.09	2.27	1.21
0016+731	121	11	2.55	1.39	1.64	0.044(2)	21.9	365	0.025(1)	8.6	0.053	0.042	0.14	0.13	1.53	1.23
0019+058	110	-56	0.77	0.42	0.44	0.031(1)	4.6	200	0.034(1)	10.0	0.269	0.399	-	0.03	0.25	0.61
0035+121	118	-50	0.83	0.77	0.38	0.007(0)	6.2	365	0.014(0)	8.2	0.008	0.039	-	-0.53	0.00	0.00
0035+413	120	-21	1.67	0.97	1.01	0.030(2)	10.0	365	0.014(1)	8.6	0.025	0.036	0.25	0.03	0.00	0.00
0055+300	125	-33	1.17	0.42	0.68	0.012(2)	12.1	365	0.016(1)	12.7	0.017	0.044	0.79	0.37	0.00	0.00
0056-001	127	-63	0.68	2.00	0.87	0.007(1)	4.8	365	0.012(0)	17.5	0.008	0.032	-	-0.63	0.32	3.75
0113-118	144	-73	0.62	1.62	1.48	0.009(1)	5.4	365	0.013(0)	20.2	0.053	0.107	-	-0.06	0.86	2.69
0123+257	133	-36	1.03	1.14	0.95	0.012(1)	10.5	365	0.013(0)	10.4	0.036	0.043	-	-0.14	0.87	0.75
0130-171	168	-76	0.62	0.77	0.59	0.013(1)	5.0	365	0.019(0)	7.6	0.030	0.072	-	-0.20	0.53	1.51
0133+476	131	-14	2.04	1.43	1.60	0.049(2)	8.6	365	0.031(1)	5.8	0.068	0.102	0.18	0.20	1.43	2.25
0134+329	134	-29	1.23	11.35	3.33	0.006(1)	9.6	365	0.012(0)	3.8	0.005	0.009	-	-0.94	0.23	1.17
0147+187	142	-42	0.88	0.44	0.45	0.022(1)	4.8	365	0.017(0)	18.3	0.053	0.102	-	0.02	0.00	0.00
0201+113	150	-48	0.78	0.91	0.73	0.014(2)	5.0	365	0.018(1)	18.1	0.010	0.099	0.14	-0.17	0.92	1.00
0202+319	141	-28	1.20	0.75	0.71	0.020(2)	6.4	365	0.021(0)	9.6	0.034	0.050	-	-0.02	0.35	0.01
0212+735	129	12	2.27	2.38	2.91	0.015(2)	11.2	365	0.019(1)	8.6	0.015	0.071	0.25	0.16	1.57	1.46
0224+671	132	6	2.52	1.59	2.11	0.032(2)	11.2	200	0.036(1)	9.9	0.124	0.186	0.34	0.16	1.21	0.46
0235+164	157	-39	0.87	1.75	2.11	0.017(1)	2.9	100	0.021(0)	5.6	0.331	0.419	-	0.09	0.72	1.06
0237-233	30	-65	0.66	4.82	1.72	0.005(1)	3.4	365	0.018(1)	5.0	0.004	0.027	-	-0.67	3.91	1.55
0256+075	169	-44	0.78	0.75	0.61	0.029(2)	7.0	365	0.037(0)	22.0	0.081	0.161	-	-0.17	0.72	0.65
0300+470	145	-10	2.13	1.43	1.51	0.066(2)	19.4	365	0.042(1)	10.5	0.085	0.088	0.25	0.12	0.95	0.47
0316+413	151	-13	1.86	33.49	30.33	0.007(1)	15.6	365	0.017(1)	5.8	0.017	0.028	-	-0.08	0.00	0.00
0319+121	171	-36	0.87	1.65	1.12	0.014(2)	7.2	365	0.013(1)	4.3	0.024	0.025	0.67	-0.30	0.94	3.48
0333+321	159	-19	1.45	2.51	1.64	0.031(2)	14.5	365	0.027(1)	6.0	0.019	0.056	0.28	-0.39	0.55	1.75
0336-019	8	-43	0.89	2.43	2.23	0.043(2)	5.3	365	0.024(0)	22.6	0.056	0.087	-	-0.02	2.27	1.58
0337+319	160	-18	1.46	0.22	0.03	0.017(1)	15.6	365	0.040(0)	6.7	0.031	0.060	-	-1.43	0.00	0.00
0355+508	150	-2	2.30	4.07	2.57	0.011(1)	24.6	365	0.034(1)	13.6	0.043	0.068	-	-0.07	1.54	4.97
0400+258	168	-20	1.34	0.99	0.77	0.016(2)	5.6	365	0.012(1)	13.9	0.022	0.032	0.36	-0.20	0.60	0.52
0403-132	206	-43	0.92	3.24	1.65	0.012(1)	5.3	365	0.021(0)	20.0	0.016	0.050	-	-0.52	0.44	0.78
0420-014	15	-33	1.10	3.55	3.50	0.030(2)	7.3	365	0.024(1)	9.6	0.069	0.099	0.11	0.13	3.10	0.74
0440-003	197	-28	1.18	1.54	0.93	0.039(2)	6.4	365	0.042(1)	28.5	0.034	0.151	0.14	-0.38	2.11	1.16
0444+634	146	12	2.00	0.43	0.59	0.065(2)	13.8	365	0.029(0)	5.9	0.116	0.196	-	0.24	0.00	0.00
0454+844	128	25	1.43	0.42	0.43	0.038(1)	5.1	365	0.026(1)	11.2	0.050	0.087	-	0.02	0.39	0.70
0500+019	198	-23	1.37	2.42	1.46	0.012(2)	7.2	365	0.010(1)	8.9	0.011	0.030	0.49	-0.38	0.00	0.00
0528+134	191	-11	1.98	2.27	3.46	0.055(2)	12.4	365	0.033(1)	5.4	0.054	0.240	0.26	0.32	2.38	1.82
0532+826	131	25	1.40	0.26	0.22	0.029(2)	5.4	365	0.034(1)	24.0	0.044	0.104	0.26	-0.12	0.00	0.00
0537-158	220	-23	1.68	0.47	0.30	0.033(2)	12.9	365	0.012(0)	9.4	0.019	0.057	-	-0.34	0.37	1.62
0538+498	162	10	1.96	15.58	4.89	0.008(1)	18.0	365	0.013(0)	11.2	0.009	0.013	-	-0.89	1.64	2.75
0552+398	172	7	2.04	3.29	7.03	0.013(2)	23.2	365	0.015(0)	9.9	0.013	0.048	-	0.40	4.00	1.38
0555-132	219	-18	2.02	0.76	0.64	0.029(2)	10.1	365	0.014(0)	4.0	0.018	0.097	-	-0.13	0.00	0.00
0615+820	132	26	1.34	0.83	0.67	0.021(2)	8.4	365	0.018(1)	10.5	0.040	0.062	0.36	-0.17	0.91	0.90
0624-058	215	-8	2.79	9.58	2.67	0.007(1)	24.5	365	0.010(0)	7.8	0.005	0.029	-	-0.98	0.00	0.00
0633+734	141	25	1.30	0.92	0.83	0.021(2)	7.1	365	0.018(1)	17.6	0.011	0.062	0.57	-0.08	0.00	0.00

TABLE 1—*Continued*

Name 1950	l deg	b deg	L_{eff} kpc	S_2 Jy	S_8 Jy	$m_2(\text{rel})$	τ_2 days	T_{sm} days	$m_8(\text{rel})$	τ_8 days	M_2	M_8	ρ	spectral index α	$S_{2,\text{vlbi}}$ Jy	Diameter mas
0650+371	179	16	1.48	1.03	0.83	0.020(2)	5.9	365	0.012(0)	3.3	0.045	0.053	-	-0.16	0.65	0.82
0653-033	216	-1	2.94	0.49	0.52	0.065(2)	16.0	365	0.039(1)	8.8	0.092	0.107	0.05	0.05	0.00	0.00
0716+714	144	28	1.18	0.44	0.60	0.046(1)	5.1	365	0.033(1)	6.7	0.102	0.248	-	0.27	0.27	0.51
0723+679	148	28	1.14	0.71	0.36	0.012(1)	10.5	365	0.022(1)	9.0	0.017	0.055	-	-0.53	0.00	0.00
0723-008	218	7	2.87	1.54	1.20	0.036(2)	4.2	365	0.018(1)	28.9	0.030	0.066	0.44	-0.19	0.99	1.26
0742+103	30	16	2.23	4.21	2.58	0.011(1)	5.3	365	0.013(0)	10.0	0.007	0.032	-	-0.32	3.85	1.39
0743+259	195	23	1.22	0.49	0.39	0.026(1)	5.6	365	0.029(0)	17.2	0.044	0.220	-	-0.18	0.46	0.52
0759+183	204	23	1.27	0.51	0.57	0.042(2)	6.5	365	0.005(0)	15.9	0.019	0.053	-	0.09	0.00	0.00
0804+499	169	32	0.94	1.10	1.25	0.022(1)	4.7	365	0.000(0)	-46.0	0.102	0.276	-	0.10	1.15	0.99
0818-128	235	13	2.57	0.85	0.60	0.045(2)	6.3	365	0.024(1)	18.2	0.049	0.084	0.58	-0.26	0.41	0.95
0827+243	200	32	0.94	0.65	0.79	0.025(2)	10.4	365	0.033(0)	29.5	0.068	0.243	-	0.14	0.46	0.75
0836+710	144	34	1.01	3.14	1.83	0.030(2)	14.0	365	0.038(1)	20.1	0.049	0.107	0.35	-0.41	1.33	0.93
0837+035	223	25	1.36	0.73	0.56	0.017(2)	5.5	365	0.004(0)	3.4	0.009	0.031	-	-0.21	0.00	0.00
0851+202	27	36	1.24	2.24	3.12	0.023(1)	6.0	150	0.029(1)	6.5	0.144	0.229	-	0.30	1.40	1.42
0859-140	242	21	1.77	2.48	1.51	0.011(1)	23.1	365	0.011(0)	6.7	0.007	0.030	-	-0.38	1.77	1.46
0922+005	232	34	1.08	0.82	0.53	0.031(1)	9.4	365	0.009(0)	9.0	0.036	0.057	-	-0.33	0.00	0.00
0923+392	4	46	1.07	4.66	10.37	0.010(1)	13.7	365	0.016(0)	25.1	0.009	0.058	-	0.39	4.97	1.22
0938+119	222	43	0.84	0.19	0.08	0.010(1)	14.4	365	0.028(0)	45.3	0.010	0.099	-	-0.65	0.00	0.00
0945+408	181	50	0.68	1.45	1.62	0.019(2)	7.2	365	0.016(1)	6.4	0.040	0.092	0.64	0.08	1.25	0.35
0952+179	217	48	0.74	1.01	0.54	0.009(1)	6.5	365	0.011(0)	23.0	0.006	0.035	-	-0.47	0.45	1.37
0954+658	146	43	0.85	0.92	0.99	0.034(2)	3.9	150	0.040(1)	4.4	0.108	0.133	0.49	0.10	0.67	1.13
1020+400	181	57	0.65	0.64	1.05	0.014(1)	7.2	365	0.011(0)	24.7	0.063	0.107	-	0.38	0.61	0.45
1022+194	218	55	0.67	0.44	0.64	0.016(1)	6.6	365	0.011(0)	8.0	0.016	0.031	-	0.30	0.00	0.00
1036-154	262	36	1.03	0.43	0.45	0.023(1)	5.0	365	0.023(1)	21.4	0.057	0.122	-	0.04	0.00	0.00
1038+528	158	55	0.69	0.29	0.71	0.032(1)	5.5	365	0.017(0)	12.6	0.072	0.127	-	0.68	0.00	0.00
1055+018	251	53	0.73	2.75	3.30	0.010(1)	6.1	365	0.015(0)	23.6	0.058	0.067	-	0.14	1.31	2.80
1100+772	130	39	0.99	0.38	0.19	0.014(2)	13.4	365	0.030(0)	5.6	0.009	0.063	-	-0.53	0.00	0.00
1116+128	242	64	0.67	1.98	1.46	0.009(1)	13.2	365	0.013(0)	7.7	0.018	0.070	-	-0.23	1.05	0.85
1123+264	211	71	0.74	1.10	1.05	0.011(1)	8.2	365	0.010(0)	5.8	0.021	0.056	-	-0.03	1.14	1.17
1127-145	275	44	0.86	4.93	2.55	0.007(1)	12.0	365	0.015(0)	7.9	0.018	0.062	-	-0.50	3.27	0.95
1128+385	175	70	0.89	0.78	0.93	0.019(1)	7.4	365	0.017(0)	25.9	0.012	0.088	-	0.13	0.64	0.80
1145-071	277	52	0.77	0.89	0.76	0.009(1)	5.9	365	0.014(0)	15.5	0.012	0.093	-	-0.12	0.78	1.57
1150+812	126	36	1.08	1.30	1.42	0.016(1)	7.5	365	0.021(1)	16.0	0.024	0.062	-	0.07	1.11	0.53
1155+251	41	78	0.80	1.22	0.70	0.005(1)	12.9	365	0.014(0)	7.2	0.016	0.027	-	-0.42	0.62	3.00
1200-051	281	55	0.76	0.41	0.50	0.015(1)	7.0	365	0.023(0)	33.8	0.058	0.188	-	0.15	0.00	0.00
1225+368	150	79	0.86	1.77	0.39	0.006(1)	18.6	365	0.011(0)	6.5	0.005	0.013	-	-1.16	0.00	0.00
1243-072	300	55	0.77	0.61	0.72	0.035(2)	12.8	365	0.014(1)	13.9	0.024	0.084	0.29	0.12	0.52	1.26
1245-197	122	43	0.94	3.74	1.27	0.003(2)	12.7	365	0.013(0)	3.3	0.001	0.019	-	-0.74	0.00	0.00
1250+568	123	61	0.71	1.62	0.45	0.007(1)	10.7	365	0.018(0)	4.9	0.009	0.033	-	-0.98	0.00	0.00
1253-055	305	57	0.77	9.32	10.89	0.008(2)	8.9	365	0.015(0)	32.1	0.020	0.070	-	0.12	7.76	1.75
1302-102	308	52	0.80	0.80	0.72	0.020(2)	7.2	365	0.023(0)	36.1	0.080	0.109	-	-0.08	1.04	0.52
1308+326	86	83	0.84	1.35	2.89	0.018(1)	4.0	365	0.016(0)	11.9	0.128	0.136	-	0.58	2.32	0.25
1328+254	22	81	0.75	5.48	2.20	0.003(1)	9.8	365	0.009(0)	2.4	0.003	0.008	-	-0.64	0.00	0.00
1328+307	56	81	0.77	11.88	5.36	0.005(1)	2.7	365	0.015(0)	3.1	0.005	0.010	-	-0.57	0.00	0.00

TABLE 1—*Continued*

Name 1950	l deg	b deg	L_{eff} kpc	S_2 Jy	S_8 Jy	$m_2(\text{rel})$	τ_2 days	T_{sm} days	$m_8(\text{rel})$	τ_8 days	M_2	M_8	ρ	spectral index α	$S_{2,\text{vltbi}}$ Jy	Diameter mas
1354+195	9	73	0.85	1.80	1.24	0.011(1)	8.6	365	0.006(0)	10.0	0.021	0.057	-	-0.29	0.00	0.00
1404+286	42	73	0.85	1.69	1.93	0.005(1)	13.0	365	0.012(0)	12.8	0.006	0.020	-	0.12	1.96	1.62
1409+524	98	61	0.73	14.06	2.07	0.005(1)	10.3	365	0.018(1)	15.9	0.006	0.035	-	-1.46	0.00	0.00
1413+135	2	66	0.90	0.85	1.31	0.005(1)	7.8	200	0.026(0)	9.0	0.016	0.230	-	0.33	0.26	1.90
1430-155	336	41	1.06	0.64	0.72	0.034(2)	6.9	365	0.014(0)	6.4	0.009	0.037	-	0.08	0.00	0.00
1438+385	66	65	0.90	0.90	0.41	0.008(1)	10.6	365	0.015(0)	17.1	0.010	0.030	-	-0.59	0.00	0.00
1449-012	353	49	1.01	0.49	0.34	0.015(1)	6.8	365	0.016(0)	4.9	0.011	0.079	-	-0.28	0.00	0.00
1455+247	35	62	0.99	0.62	0.26	0.004(0)	11.6	365	0.013(0)	3.0	0.004	0.014	-	-0.66	0.00	0.00
1502+106	11	55	1.02	1.89	1.55	0.028(2)	10.0	200	0.016(0)	2.8	0.070	0.114	-	-0.11	1.64	0.34
1511+238	35	58	1.02	1.37	0.54	0.004(0)	14.3	365	0.011(0)	23.6	0.005	0.018	-	-0.65	0.00	0.00
1514+197	28	56	1.03	0.54	0.68	0.075(2)	6.7	365	0.021(1)	11.5	0.089	0.141	0.49	0.18	0.47	1.83
1525+314	49	56	1.03	0.77	0.42	0.008(0)	3.2	365	0.021(0)	18.4	0.013	0.018	-	-0.46	0.00	0.00
1538+149	24	49	1.09	1.26	0.93	0.043(2)	8.4	365	0.031(1)	18.6	0.033	0.052	0.38	-0.24	0.56	1.48
1547+508	80	49	0.91	0.70	1.18	0.011(0)	3.6	365	0.017(0)	3.0	0.005	0.065	-	0.39	0.00	0.00
1555+001	10	38	1.19	0.97	1.12	0.036(2)	7.7	365	0.023(1)	17.1	0.091	0.094	0.33	0.04	1.02	1.05
1611+343	55	47	1.08	3.29	3.24	0.014(1)	10.1	365	0.015(1)	17.9	0.026	0.042	-	-0.07	4.16	2.11
1614+051	18	36	1.22	0.63	0.64	0.033(2)	16.3	365	0.015(0)	6.0	0.033	0.053	-	0.02	0.68	1.07
1624+416	66	44	1.03	1.60	1.01	0.007(1)	8.2	365	0.012(0)	20.7	0.019	0.026	-	-0.35	0.82	0.99
1635-035	13	27	1.42	0.39	0.33	0.066(2)	17.8	365	0.029(1)	7.9	0.047	0.063	0.56	-0.13	0.00	0.00
1641+399	63	41	1.11	7.55	7.95	0.012(2)	14.1	365	0.014(0)	3.2	0.046	0.123	-	0.14	5.14	1.48
1655+077	27	29	1.40	1.07	0.97	0.021(2)	16.0	365	0.024(1)	6.0	0.056	0.090	0.54	-0.08	0.68	2.02
1656+477	74	39	1.18	1.22	1.24	0.024(2)	13.2	365	0.011(0)	3.4	0.011	0.020	-	0.01	1.06	0.52
1741-038	22	13	2.45	2.03	2.59	0.097(2)	18.2	365	0.027(1)	7.4	0.070	0.058	0.19	0.19	1.77	0.70
1742-289	173	0	2.18	0.46	0.81	0.049(1)	4.3	365	0.056(1)	14.1	0.025	0.062	-	0.51	0.00	0.00
1749+096	35	18	2.19	1.14	2.40	0.059(2)	8.0	150	0.036(2)	5.9	0.155	0.264	0.21	0.48	1.48	0.43
1749+701	101	31	1.39	0.73	0.62	0.030(2)	9.4	365	0.033(1)	15.2	0.078	0.126	0.60	-0.11	0.61	2.11
1756+237	49	22	2.00	0.81	0.59	0.032(2)	7.7	365	0.014(1)	6.2	0.012	0.029	0.40	-0.24	0.00	0.00
1803+784	110	29	1.39	2.23	2.87	0.026(2)	6.5	365	0.027(1)	12.2	0.058	0.073	0.40	0.19	1.63	1.37
1807+698	100	29	1.46	1.47	1.75	0.015(2)	10.4	365	0.020(1)	12.6	0.020	0.061	0.65	0.18	0.79	1.99
1821+107	39	11	3.35	1.11	0.75	0.034(2)	15.7	365	0.021(1)	6.2	0.019	0.031	0.56	-0.26	1.29	0.60
1823+568	86	26	1.74	1.18	1.38	0.029(2)	5.2	365	0.016(1)	10.0	0.019	0.091	0.63	0.12	0.84	0.61
1828+487	77	24	1.97	8.31	3.54	0.008(1)	14.1	365	0.011(0)	10.9	0.007	0.046	-	-0.65	0.00	0.00
1830+285	57	17	2.70	0.47	0.53	0.046(2)	10.7	365	0.018(1)	6.5	0.050	0.068	0.33	0.08	0.48	2.43
1928+738	106	24	1.70	3.75	4.00	0.015(1)	11.4	365	0.017(0)	8.9	0.019	0.033	-	0.05	0.00	0.00
1943+228	59	-1	8.37	0.31	0.16	0.020(1)	21.0	365	0.031(0)	4.8	0.026	0.064	-	-0.52	0.00	0.00
1944+251	61	0	8.51	0.32	0.10	0.014(1)	11.1	365	0.080(0)	4.4	0.015	0.133	-	-0.89	0.27	3.05
1947+079	47	-9	4.13	1.30	0.72	0.021(2)	18.6	365	0.008(0)	14.0	0.015	0.028	-	-0.45	0.00	0.00
2005+403	77	4	2.86	2.79	3.31	0.007(1)	3.9	365	0.037(2)	11.8	0.033	0.032	-	0.05	0.87	1.25
2007+776	110	23	1.71	1.41	2.35	0.045(2)	7.5	365	0.037(1)	17.5	0.093	0.151	0.20	0.39	3.01	14.10
2008-068	36	-21	1.91	2.21	0.78	0.011(0)	5.6	365	0.019(0)	11.8	0.009	0.045	-	-0.80	0.00	0.00
2032+107	55	-17	2.59	0.84	0.54	0.021(2)	7.6	200	0.025(1)	7.5	0.088	0.178	0.14	-0.34	0.00	0.00
2037+511	89	6	4.59	4.93	4.09	0.016(2)	27.5	365	0.024(1)	8.8	0.029	0.072	-0.12	-0.14	0.00	0.00
2047+098	57	-21	2.19	0.49	0.64	0.031(2)	5.8	365	0.018(0)	13.5	0.046	0.150	-	0.21	2.03	1.66
2059+034	53	-27	1.66	0.68	0.96	0.054(1)	11.7	365	0.021(0)	6.8	0.062	0.212	-	0.27	0.00	0.00

TABLE 1—*Continued*

Name 1950	l deg	b deg	L_{eff} kpc	S_2 Jy	S_8 Jy	$m_2(\text{rel})$	τ_2 days	T_{sm} days	$m_8(\text{rel})$	τ_8 days	M_2	M_8	ρ	spectral index α	$S_{2,\text{vlbi}}$ Jy	Diameter mas
2105+420	85	-3	5.27	1.48	0.75	0.006(0)	18.0	365	0.014(0)	18.9	0.009	0.042	-	-0.52	0.78	0.72
2113+293	77	-13	3.26	0.85	0.87	0.049(2)	7.1	365	0.027(0)	5.3	0.126	0.178	-	0.02	0.00	0.00
2121+053	58	-30	1.50	2.26	1.72	0.047(2)	8.5	365	0.038(0)	27.4	0.088	0.114	-	-0.21	0.84	0.85
2134+004	55	-36	1.24	6.94	6.95	0.019(2)	9.4	365	0.014(0)	12.3	0.009	0.029	-	0.00	0.95	0.94
2155-152	41	-48	0.88	2.70	2.00	0.022(1)	12.4	365	0.019(0)	5.3	0.074	0.066	-	-0.23	8.64	1.60
2200+420	92	-10	3.43	3.08	3.40	0.031(2)	7.8	100	0.022(2)	4.7	0.225	0.309	0.66	0.09	2.66	1.64
2209+081	70	-37	1.21	0.82	0.24	0.011(1)	9.9	365	0.024(0)	11.7	0.013	0.097	-	-0.93	3.27	0.71
2214+350	90	-18	2.39	0.47	0.57	0.085(2)	6.5	365	0.029(1)	6.6	0.087	0.076	0.48	0.14	0.00	0.00
2234+282	90	-26	1.72	1.69	1.64	0.041(2)	7.9	365	0.021(0)	9.0	0.088	0.103	-	0.00	0.00	0.00
2251+158	86	-38	1.18	12.45	10.04	0.013(1)	8.0	365	0.019(0)	13.8	0.067	0.169	-	-0.09	1.68	1.07
2251+244	91	-31	1.43	1.49	0.53	0.008(1)	5.4	365	0.000(0)	7.9	0.005	0.031	-	-0.80	0.00	0.00
2307+107	87	-45	1.00	0.37	0.36	0.025(1)	3.1	365	0.022(0)	15.7	0.052	0.130	-	-0.02	0.00	0.00
2319+272	100	-31	1.37	0.80	0.58	0.017(1)	5.1	365	0.015(0)	29.2	0.033	0.061	-	-0.24	0.00	0.00
2344+092	97	-50	0.87	1.68	1.19	0.008(1)	7.3	365	0.013(0)	14.7	0.012	0.059	-	-0.26	0.76	1.78
2352+495	114	-12	2.58	2.18	1.09	0.016(2)	9.2	365	0.016(0)	7.3	0.010	0.016	-	-0.49	1.02	0.89

REFERENCES

- Armstrong, J. W., Rickett, B. J., & Spangler, S. R. 1995, ApJ, 443, 209
- Bignall, H. E., Jauncey, D. L., Lovell, J. E. J., Tzioumis, A. K., Kedziora-Chudczer, L., Macquart, J.-P., Tingay, S. J., Rayner, D. P., Clay, R. W. 2003, ApJ, 585, 653
- Blandford, R. D. & Königl, A. 1979, ApJ, 232, 34
- Blandford, R. D., Narayan, R. & Romani, R. W. 1986, ApJ, 301, L53
- Coles, W. A., Frehlich, R. G., Rickett, B. J., & Codona, J. L. 1987, ApJ, 315, 666 (CFRC)
- Coles, W. A. 1988, in "Radio wave scattering in the interstellar medium", Proceedings of the AIP Conference, San Diego, Jan., 1988, p. 163.
- bibitem[]108 Cordes, J. M. & Lazio, T. J. W. 2005, astro-ph/0207156 (v3)
- Dennett-Thorpe, J. & de Bruyn, A. G. 2000, ApJ, 529, L65
- Dennett-Thorpe, J. & de Bruyn, A. G. 2002, Nature, 415, 57
- Dennett-Thorpe, J. & de Bruyn, A. G., 2003, A&A, 403, 113
- Dennison, B. & Condon, J. J. 1981, ApJ, 246, 835
- Dennison, B., Fiedler, R. L., Johnston, K. J., Spencer, J. H., Waltman, E. B., Angerhofer, P. E., Florkowski, D. R., Josties, F. J., Klepczynski, W. J., McCarthy, D. D. & Matzakakis, D. N. 1987, ApJ, 313, 141
- Dent, W. A. 1965, *Science*, 146, 1458
- Desai, K. M. & Fey, A. L. 2001, ApJS, 133, 395
- Fanti, C., Fanti, R., Ficarra, A., Mantovani, F., Padrielli, L., Weiler, K. W. 1981, A&AS, 45, 61
- Fey, A. L. & Charlot, P. 1997, ApJS, 111, 95
- Fey, A. L. & Charlot, P. 2000, ApJS, 128, 17
- Fiedler, R. L., Dennison, B., Johnston, K. J., & Hewish, A. 1987a, Nature, 326, 675
- Fiedler, R. L. et al. 1987b, ApJS, 65, 319 (F87)
- Fiedler, R. L., Dennison, B., Johnston, K. J., Waltman, E. B. & Simon, R. S. 1994, ApJ, 430, 581
- Haffner, L. M., Reynolds, R. J., Tufte, S. L., Madsen, G. J., Jaehnig, K. P., Percival, J. W. 2003, ApJS, 149, 405.
- Heeschen, D. S. 1984, AJ, 89, 1111
- Hjellming, R. M. & Narayan, R., 1986, ApJ, 310, 768
- Hughes, P. A., Aller, H. D. and Aller, M. F. 1992, ApJ, 396, 469
- Ishimaru, A., 1978, *Wave Propagation and Scattering in Random Media*, Academic Press, New York
- Jauncey, D.L. and Macquart, J.-P. 2001, A&A, 370, L9
- Jauncey, D. L., Johnston, H. M., Bignall, H. E., Lovell, J. E. J., Kedziora-Chudczer, L., Tzioumis, A. K. and Macquart, J.-P. Ap&SS, 2003, 288, 68
- Kedziora-Chudczer, L., Jauncey, D. L., Wieringa, M. H., Walker, M. A., Nicolson, G. D., Reynolds, J. E. and Tzioumis, A. K. 1997, ApJ, 490, L9-12
- Kellermann, K. I. and Pauliny-Toth, I. 1968, ARA&A, 6, 417
- Kellermann, K. I. and Pauliny-Toth, I. 1981, ARA&A, 19, 373
- Kraus, A., Quirrenbach, A., Lobanov, A. P., Krichbaum, T. P., Risse, M., Schneider, P., Qian, S. J., Wagner, S. J., Witzel, A., Zensus, J. A., Heidt, J., Bock, H., Aller, M., Aller, H. 1999, A&A, 344, 807
- Lazio, T. Joseph W.; Fey, A. L.; Dennison, Brian; Mantovani, F.; Simonetti, J. H.; Alberdi, Antonio; Foley, A. R.; Fiedler, R.; Garrett, M. A.; Hirabayashi, Hisashi; Jauncey, D. L.; Johnston, K. J.; Marcaide, Jon; Migenes, Victor; Nicolson, G. D.; Venturi, Tiziana 2000, ApJ, 534, 706
- Lazio, T. J. W., Waltman, E. B., Ghigo, F. D., Fiedler, R. L., Foster, R. S. & Johnston, K. J. 2001 ApJS, 136, 265 (L01)

- Lovell, J.E.J., Jauncey,D.L., Bignall,H.E., Kedziora-Chudczer, L., Macquart, J-P., Rickett, B.J., Tzioumis, A.K. 2003, AJ, 126, 1699.
- Medd, W. J., Andrew, B. H., Harvey, G. A. and Locke, J. L. 1972, MmRAS, 77, 109
- Narayan, R. 1992, Phil. Trans. R. Soc. London A, 341, 151
- Peng, B. and de Bruyn, A. G. 2004, ApJ, 610, 151
- Quirrenbach, A., Witzel, A., Kirchbaum, T. P., Hummel, C. A., Wegner, R., Schalinski, C. J., Ott, M., Alberdi, A., Rioja, M. 1992, A&A, 258, 279
- Quirrenbach, A., et al. 2000, A&A Suppl., 141, 2212
- Readhead, A. C. S., 1994, ApJ, 426, 51
- Rickett, B. J. 1977, ARA&A, 15, 479
- Rickett, B. J. 1986, ApJ, 307, 564
- Rickett, B. J., Coles, W.A., & Bourgois, G. 1984, A&A, 134, 390
- Rickett, B. J. 1990, ARA&A, 28, 561
- Rickett, B. J., Quirrenbach, A., Wegner, R., Krichbaum, T. P. & Witzel A. 1995, A&A, 293, 479
- Rickett, B. J., Witzel A., Kraus, A., Krichbaum,T. P. and Qian, S.J. 2001, ApJ, 550, L11-14
- Rickett, B. J., Kedziora-Chudczer, L. & Jauncey, D. L. 2002. ApJ, 581, 103
- Shapirovskaia, N. Y. 1978, *Sov. Astron. AJ* , 22, 544
- Sieber, W. 1982, A&A, 113, 311
- Snowden, S.L., Egger, R., Finkbeiner, D.P., Freyburg, M. J. & Plucinsky, P. P. 1998, ApJ, 493, 715
- Spangler, S. R., Eastman, W. A., Gregorini, L., Mantovani, F. & Padrielli, L. 1993, A&A, 267, 213
- Stevens, J. A., Litchfield, S. J., Robson, E. I., Hughes, D. H., Gear, W. K., Terasranta, H., Valtaoja, E., Tornikoski, M. 1994, ApJ, 437, 91
- Tsutsumi, T. and Duric, N., 1999, *Advances in Space Research*, 23, 1013
- Taylor, J. H., & Cordes, J. M. 1993, ApJ, 411, 674
- Wagner, S.J., Witzel, A., Heidt, J., Krichbaum, T.P., Qian, S.J., Quirrenbach, A., Wegner, R., Aller, H. & M., Anton, K., Appenzeller, I., Eckart, A., Kraus, A., Naundorf, C., Kneer, R., Steffen, W. & Zensus, J.A. 1996, AJ, 111, 2187
- Walker, M. A. 1998, MNRAS, 294, 307
- Walker, M. A. 2001, MNRAS, 321, 176
- Waltman, E. B., , Fiedler, R. L., Johnston, K. J., Spencer, J. H., Florkowski, D. R., Josties, F. J., McCarthy, D. D. & Matsakis, D. N 1991, 1991 ApJS, 77, 379 (W91)